GVTDOC
D 211.
9:
3748

0017430 54

NAVAL SHIP RESEARCH AND DEVELOPMENT CENTER
Bethesda, Maryland 20034

LAMINAR FLOWS PAST ELLIPTIC CYLINDERS AT VARIOUS ANGLES OF ATTACK

LAMINAR FLOWS PAST ELLIPTIC CYLINDERS AT VARIOUS ANGLES OF ATTACK

Hans J. Lugt and Henry J. Haussling

Approved for public release; distribution unlimited.

COMPUTATION AND MATHEMATICS DEPARTMENT
RESEARCH AND DEVELOPMENT REPORT

20070119077

February 1972 Report 3748

The Naval Ship Research and Development Center is a U. S. Navy center for laboratory effort directed at achieving improved sea and air vehicles. It was formed in March 1967 by merging the David Taylor Model Basin at Carderock, Maryland with the Marine Engineering Laboratory at Annapolis, Maryland.

Naval Ship Research and Development Center
Bethesda, Md. 20034

MAJOR NSRDC ORGANIZATIONAL COMPONENTS

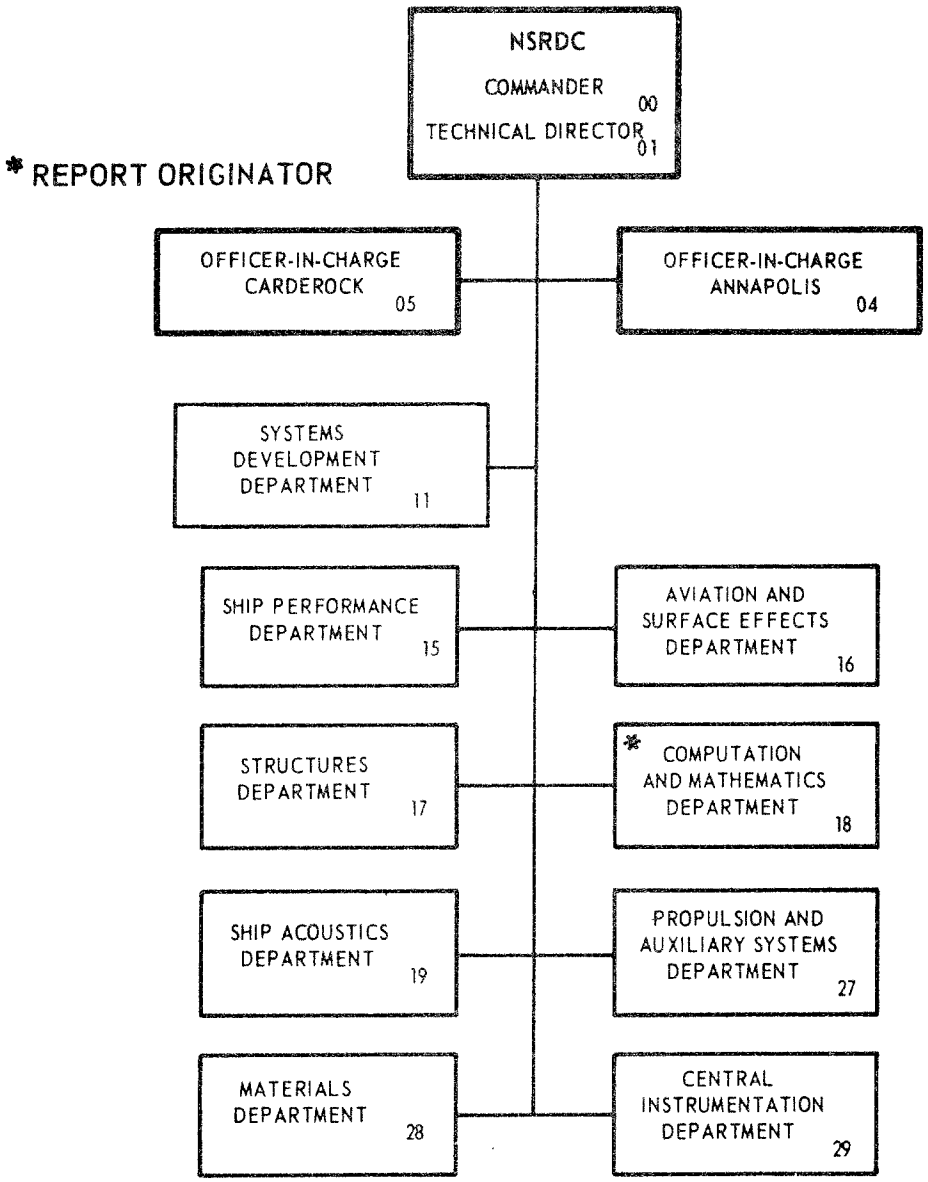

NDW-NSRDC 3960/44 (REV. 8/71)
GPO 917-872

DEPARTMENT OF THE NAVY
NAVAL SHIP RESEARCH AND DEVELOPMENT CENTER
Bethesda, Maryland 20034

LAMINAR FLOWS PAST ELLIPTIC CYLINDERS AT VARIOUS ANGLES OF ATTACK

by

Hans J. Lugt and Henry J. Haussling

Approved for public release; distribution unlimited.

February 1972 Report 3748

TABLE OF CONTENTS

	Page
ABSTRACT	1
ADMINISTRATIVE INFORMATION	1
INTRODUCTION	2
FORMULATION OF THE PROBLEM	3
NUMERICAL ANALYSIS	7
RESULTS	20
CONCLUSIONS	41
ACKNOWLEDGMENT	47
REFERENCES	48

LIST OF FIGURES AND TABLES

Figure 1 -	Elliptic coordinate system and definition of angle of attack	4
Figure 2 -	Elliptic grid system near the body, $\eta_1 = 0.1$, $\Delta\eta = 0.05$, $\Delta\theta = \pi/30$. The total number of grid points is 75 x 60 = 4500	9
Figure 3 -	Grid near the tip	10
Figure 4 -	Drag coefficient versus time for Re = 10, $\alpha = 90^{\circ}$, $\eta_1 = 0.1$	22
Figure 5 -	Streamlines for Re = 10, $\alpha = 90^{\circ}$, $\eta_1 = 0.1$ at t = 11.2 (almost steady state)	23

Page

Figure 6 - Lines of constant vorticity for Re = 10, $\alpha = 90^{\circ}$, $\eta_1 = 0.1$ at t = 11.2 (almost steady state). 24

Figure 7 - Dimensionless wake length versus time for Re = 10 and 50, $\alpha = 90^{\circ}$, $\eta_1 = 0.1$ 25

Figure 8 - Sequence of streamlines in the initial phase of wake development for Re = 50, $\alpha = 90^{\circ}$, $\eta_1 = 0.1$ 27

Figure 9 - Sequence of streamlines and equal-vorticity lines for Re = 200, $\alpha = 45^{\circ}$, $\eta_1 = 0.1$ at various times after the abrupt start. Potential flow at t = 0. 29

Figure 10 - Sequence of streamlines and equal-vorticity lines for the third cycle of Re = 200, $\alpha = 45^{\circ}$, $\eta_1 = 0.1$ after the abrupt start. 30

Figure 11 - Some patterns of streamlines and equal-vorticity lines of the entire wake region for Re = 200, $\alpha = 45^{\circ}$, $\eta_1 = 0.1$ during the third cycle. 31

Figure 12 - Drag, lift, and moment coefficients versus time for Re = 200, $\alpha = 45^{\circ}$, $\eta_1 = 0.1$. 32

Figure 13 - Coefficients for frictional drag and lift versus time for Re = 200, $\alpha = 45^{\circ}$, $\eta_1 = 0.1$. 34

Figure 14 - Surface vorticity versus θ for the third cycle of Re = 200, $\alpha = 45^{\circ}$, $\eta_1 = 0.1$. 35

Figure 15 - Surface pressure versus θ for the third cycle of Re = 200, $\alpha = 45^{\circ}$, $\eta_1 = 0.1$. 36

Figure 16 - Decay of central vorticity of the initial vortex for Re = 200, $\alpha = 45^{\circ}$, $\eta_1 = 0.1$. 38

Page

Figure 17 - Some patterns of streamlines and equal-vorticity lines for Re = 200, $\alpha = 10^{\circ}$, $\eta_1 = 0$ after the abrupt start..... 39

Figure 18 - Drag, lift, and moment coefficients versus time for Re = 200, $\alpha = 10^{\circ}$, $\eta_1 = 0$ after the abrupt start..... 40

Figure 19 - Sequence of streamlines and equal vorticity lines for Re = 30, $\alpha = 45^{\circ}$, $\eta_1 = 0.1$ at various times after the abrupt start. Potential flow at t = 0..... 42

Figure 20 - Coefficients for frictional drag and lift versus time for Re = 30, $\alpha = 45^{\circ}$, $\eta_1 = 0.1$ after the abrupt start..... 43

Figure 21 - Some patterns of streamlines and equal-vorticity lines for Re = 15, $\alpha = 45^{\circ}$, $\eta_1 = 0.1$ after the abrupt start..... 44

Figure 22 - Drag, lift, and moment coefficients versus time for Re = 15, $\alpha = 45^{\circ}$, $\eta_1 = 0.1$ after the abrupt start..... 45

Figure 23 - Coefficients for frictional drag and lift versus time for Re = 15, $\alpha = 45^{\circ}$, $\eta_1 = 0.1$ after the abrupt start..... 46

Table 1 - Compilation of the Calculated Examples 21

Table 2 - Drag Coefficients for Symmetric Flow Configurations .. 26

NOTATION

a	Focal distance
C_D	Drag coefficient
C_{DF}, C_{DP}	Drag coefficients due to friction and pressure
C_L	Lift coefficient
C_{LF}, C_{LP}	Lift coefficients due to friction and pressure
C_M	Moment coefficient
C_{MF}, C_{MP}	Moment coefficients due to friction and pressure
d	Width $= 2a \cosh \eta_1$
h^2	$= \cosh^2 \eta - \cos^2 \theta$
i^2	$= -1$
i, j	Location of grid point
J	Jacobian
L	Number of points in the η-direction
M	Number of points in the θ-direction
n	Frequency of vortex shedding
p'	Pressure
p	Dimensionless pressure $= p'/\rho U^2$
r, ϕ	Polar coordinates
Re	Reynolds number $= 2aU/\nu$
Re_d	Reynolds number $= dU/\nu$
s	Length of wake
St	Strouhal number $= dn/U$
t'	Time

t	Dimensionless time = $t'U/a$
t_0	Start of vortex decay
$\vec{U}$	Velocity vector at $\eta = \infty$
U	Magnitude of $\vec{U}$
$\vec{v}'$	Velocity vector
v'_r, v'_ϕ	Velocity components corresponding to r, ϕ
$\vec{v}$	Dimensionless velocity vector = $\vec{v}'/U$
v_η, v_θ	Dimensionless velocity components corresponding to η, θ
x, y	Cartesian coordinates
α	Angle of attack
ϵ	Upper bound in the criterion (24)
η, θ	Elliptic coordinates defined by Equation (1)
$\Delta\eta, \Delta\theta$	Space increments
Δt	Time increment
ν	Kinematic viscosity of the fluid
ρ	Density of the fluid
ψ'	Stream function
ψ	Dimensionless stream function = ψ'/aU
$\vec{\omega}'$	Vorticity vector
$\vec{\omega}$	Dimensionless vorticity vector = $\vec{\omega}'U/a$
ω	Vorticity component normal to the (x, y)-plane

Subscripts

1	Surface of the body
2, 3	$\Delta\eta$, $2\Delta\eta$ from the surface

i, j	Location of grid point
L	Outer boundary

Superscripts

k	Number of iterations
n	Time step

ABSTRACT

Numerical solutions for laminar incompressible fluid flows past thin elliptic cylinders at various angles of attack are obtained using a stream function-vorticity formulation. The flow is considered to be two-dimensional and time-dependent. Potential flow is selected as the initial condition. Almost steady-state solutions have been computed for the cases $\alpha = 0^{\circ}$, Re = 200; $\alpha = 45^{\circ}$, Re = 15; and $\alpha = 90^{\circ}$, Re = 10 where α and Re are the angle of attack and the Reynolds number, respectively. Vortex shedding has been studied for $\alpha = 45^{\circ}$, Re = 30 and 200.

ADMINISTRATIVE INFORMATION

This study was funded in part by the Naval Material Command under the Independent Research Program, Task Area ZR 011 01 01, and in part by the Naval Ship Systems Command under the Mathematical Sciences Program, Subproject SR 014 03 01. The date of completion was December 1971.

A condensed version of this paper was published under the title "Laminar Flows Past a Flat Plate at Various Angles of Attack" in the Proceedings of the Second International Conference on Numerical Methods in Fluid Dynamics, September 15-19, 1970, University of California, Berkeley. Lecture notes in Physics 8, Springer-Verlag, 1971, p. 78.

INTRODUCTION

Flows past a finite flat plate of infinite span in a channel or in an infinite body of fluid have been studied numerically by a number of investigators[1-7]. In all these studies the angle of attack α is either 0° or 90° except for work reported in a recent paper[7], in which the steady flow past an infinitely thin plate between two parallel walls with $\alpha = 45^{\circ}$ was investigated. Only the work by Fromm and Harlow[2] considers vortex shedding from a plate. The angle of attack is $\alpha = 90^{\circ}$ in this case.

Periodic vortex shedding from a circular cylinder has been the subject of recent numerical studies[8-11]. Extensive surveys on experimental as well as theoretical work on periodic vortex shedding from bodies were presented by von Krzywoblocki[12] and Morkovin[13].

Numerical studies on flows around plates, which have high surface curvature at the tips, pose many more difficulties and demand much more computer time than studies on motions past circular cylinders. The analytical and numerical problems involved have been investigated and discussed elsewhere[14-17] for wedges, cones, and disk-shaped bodies.

The objective of the present study is the numerical investigation of flows past inclined plates, especially the flow characteristics of vortex shedding. Due to the high computer costs involved, the study was limited essentially to the Reynolds numbers 10, 15, 30 and 200.

---

1 References are listed on page 48.

FORMULATION OF THE PROBLEM

The laminar flow of an incompressible fluid past a plate of elliptic cross-section was considered. The motion was assumed to be two-dimensional and time-dependent. Mathematically, an initial-boundary value problem for the Navier-Stokes equations must be solved. This is conveniently carried out in the elliptic coordinate system (η, θ) (see Figure 1) which is defined by the transformation:

$$x + iy = a \cosh(\eta + i\theta), \quad a > 0, \; i^2 = -1 . \tag{1}$$

The focal distance is designated by a. The equations of motion are formulated in terms of ψ, the dimensionless stream function, and ω, the dimensionless vorticity component normal to the (η, θ)-plane:

$$\frac{\partial \omega}{\partial t} + \frac{1}{h^2} \frac{\partial(\psi, \omega)}{\partial(\eta, \theta)} = \frac{2}{Re} \nabla^2 \omega , \tag{2}$$

$$\nabla^2 \psi = \omega . \tag{3}$$

Here, t and Re are dimensionless time and Reynolds number $Re = 2aU/\nu$, where ν is the kinematic viscosity and U the magnitude of the constant velocity at infinity. (Sometimes, the Reynolds number $Re_d = dU/\nu$ with $d = 2a\cosh\eta_1$ is used for practical reasons. In all cases considered in this paper, except for $\eta_1 = 0.2$, $Re \approx Re_d$.) The characteristic length and velocity scales in the dimensionless quantities are a and U. In particular, the del operator is made dimensionless by a. The coefficient h is defined by $h^2 = \cosh^2\eta - \cos^2\theta$.

The contour of the plate is the constant coordinate line $\eta = \eta_1$ (Figure 1). On this line boundary conditions are prescribed such that the velocity vector $\vec{v}$ is zero. The dimensionless velocity components

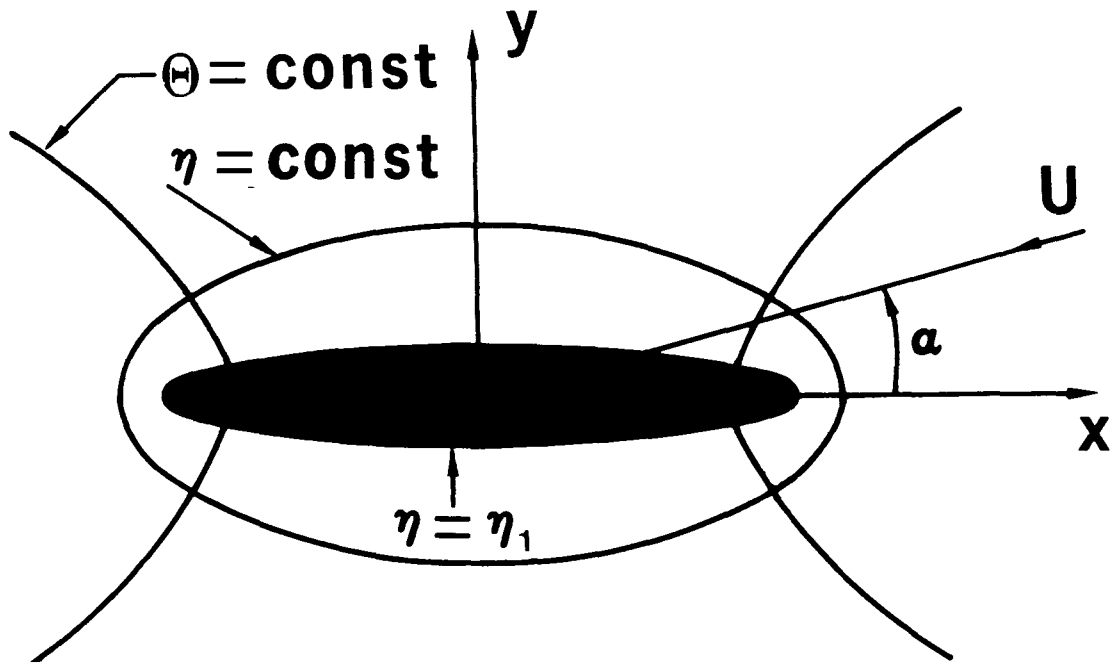

Figure 1 - Elliptic coordinate system and definition of angle of attack

v_η and v_θ are connected with ψ by

$$v_\eta = -\frac{1}{h}\frac{\partial\psi}{\partial\theta}, \quad v_\theta = \frac{1}{h}\frac{\partial\psi}{\partial\eta} . \tag{4}$$

Thus, at the body surface the boundary conditions are

$$\eta = \eta_1: \quad \psi = 0, \quad \frac{\partial\psi}{\partial\eta} = 0 . \tag{5}$$

Here, the constant value of ψ is chosen to be zero. Far away from the plate, a uniform parallel flow with velocity $\vec{U}$ is assumed, where the vector $\vec{U}$ is specified by α and U (Figure 1). In terms of ψ the conditions are:

$$\eta = \infty: \quad \frac{\partial\psi}{\partial\eta} = h\sin(\theta - \alpha), \quad \frac{\partial\psi}{\partial\theta} = h\cos(\theta - \alpha) . \tag{6}$$

Potential flow is taken to be the initial condition.

In order to compute drag, lift, and torque on the plate by means of flow quantities at the body, the pressure distribution on the surface of the plate must be determined. From the Navier-Stokes equations it follows that

$$\nabla p = -\frac{2}{Re}\,\mathrm{curl}\,\vec{\omega} - \frac{\partial\vec{v}}{\partial t} - \nabla\left(\frac{\vec{v}^2}{2}\right) + \vec{v} \times \vec{\omega} , \tag{7}$$

where $\vec{\omega}$ is the dimensionless vorticity vector, and where the pressure is made dimensionless by ρU^2. The quantity ρ is the density of the fluid. The surface pressure is computed from the θ-component of (7) to be

$$p_1 = p_c + \frac{2}{Re}\int_{\frac{\pi}{2}}^{\theta}\left(\frac{\partial\omega}{\partial\eta}\right)_1 d\bar{\theta} , \tag{8}$$

where p_c is the pressure at $(\eta_1, \frac{\pi}{2})$. This point is selected for numerical reasons. The pressure p_c is obtained from the η-component of (7) by prescribing the value of p at $\eta = \infty$ to be $p_\infty = 0$:

$$p_c = \int_{\eta_1}^{\infty} \left[\frac{2}{Re} \frac{\partial \omega}{\partial \theta} + h \frac{\partial v_\eta}{\partial t} - h v_\theta \omega \right] d\eta + \frac{1}{2} . \tag{9}$$

The drag coefficient is defined by

$$C_D = \text{Drag}/\tfrac{\rho}{2} U^2 \, a \cosh \eta_1 \tag{10}$$

and consists of two parts, the drag coefficients due to pressure and friction $C_D = C_{DP} + C_{DF}$, with

$$C_{DP} = -2 \tanh \eta_1 \cos \alpha \int_0^{2\pi} p_1 \cos \theta \, d\theta - 2 \sin \alpha \int_0^{2\pi} p_1 \sin \theta \, d\theta , \tag{11}$$

$$C_{DF} = \frac{4}{Re} \left[-\cos \alpha \int_0^{2\pi} \omega_1 \sin \theta \, d\theta + \tanh \eta_1 \sin \alpha \int_0^{2\pi} \omega_1 \cos \theta \, d\theta \right], \tag{12}$$

Equation (11) is simplified by means of Equation (8) to

$$C_{DP} = \frac{4}{Re} \left[\tanh \eta_1 \cos \alpha \int_0^{2\pi} \left(\frac{\partial \omega}{\partial \eta} \right)_1 \sin \theta \, d\theta \right.$$

$$\left. - \sin \alpha \int_0^{2\pi} \left(\frac{\partial \omega}{\partial \eta} \right)_1 \cos \theta \, d\theta \right] . \tag{13}$$

Correspondingly, the lift coefficient is

$$C_L = \text{Lift}/\tfrac{\rho}{2} U^2 \, a \cosh \eta_1 \tag{14}$$

with

$$C_{LP} = \frac{4}{Re} \left[- \tanh \eta_1 \sin \alpha \int_0^{2\pi} \left(\frac{\partial \omega}{\partial \eta}\right)_1 \sin \theta \, d\theta \right.$$

$$\left. - \cos \alpha \int_0^{2\pi} \left(\frac{\partial \omega}{\partial \eta}\right)_1 \cos \theta \, d\theta \right], \tag{15}$$

$$C_{LF} = \frac{4}{Re} \left[\sin \alpha \int_0^{2\pi} \omega_1 \sin \theta \, d\theta + \tanh \eta_1 \cos \alpha \int_0^{2\pi} \omega_1 \cos \theta \, d\theta \right]. \tag{16}$$

The moment coefficient is

$$C_M = \text{Torque}/\frac{\rho}{2} U^2 a^2 \cosh^2 \eta_1 \tag{17}$$

with

$$C_{MP} = \frac{2}{Re \cosh^2 \eta_1} \int_0^{2\pi} \left(\frac{\partial \omega}{\partial \eta}\right)_1 \sin^2 \theta \, d\theta \ , \tag{18}$$

$$C_{MF} = \frac{4}{Re} \tanh \eta_1 \int_0^{2\pi} \omega_1 \, d\theta \ . \tag{19}$$

NUMERICAL ANALYSIS

The infinite domain of integration in the (η, θ)-plane is replaced by a finite network of points $(\eta_1 + (i-1)\Delta\eta, \ (j-1)\Delta\theta)$ with $i = 1, \ldots L$, $j = 1, \ldots M$. For most examples, L and M are 75 and 60; that is, the total number of grid points is 4500 and $\Delta\theta = \pi/30$. In special instances $M = 80$ (or $\Delta\theta = \pi/40$) is used. For all cases $\Delta\eta = 0.05$. This choice

is based on previous experience[16, 18]. With $\Delta\eta = 0.05$ and $L = 75$, the outer boundary $\eta = \eta_L = \eta_1 + (L-1)\Delta\eta$ is about 11 plate lengths away from the body center. Figure 2 shows the grid system in the vicinity of the plate for $\eta_1 = 0.1$. Two different layouts are used: one which includes the tip points in the grid, another which excludes the tip points by shifting the grid $\Delta\theta/2$ in the θ-direction (see Figure 3). The importance of this distinction was noticed in the course of the study when numerical computations revealed a much larger stability for plates with high curvature ($\eta_1 < 0.1$) when the tip points were excluded from the grid. A detailed account was given in an earlier report[17].

The numerical solution of the initial boundary value problem stated in the previous section poses two essential difficulties: the approximation of the differential operators of Equations (2) and (3) through suitable difference schemes, and the prescription of boundary conditions for the outer boundary, where $\eta_L < \infty$ in the numerical scheme.

The discretization of the differential operators is similar to that used by Rimon[18]. The linear part of Equation (2) is approximated by the DuFort-Frankel scheme. The Jacobian is written in conservation form and expressed by central difference formulae. Then, Equation (2) yields, when solved for the $(n+1)^{th}$ time step of $\omega_{i,j}$,

$$\omega_{i,j}^{n+1} = \left[\frac{1}{2\Delta t} + \frac{2}{Re\, h_{i,j}^2}\left(\frac{1}{(\Delta\eta)^2} + \frac{1}{(\Delta\theta)^2}\right)\right]^{-1} \left[\frac{\omega_{i,j}^{n-1}}{2\Delta t}\right.$$

$$+ \frac{2}{Re\, h_{i,j}^2}\left\{\frac{1}{(\Delta\eta)^2}(\omega_{i+1,j}^{n} - \omega_{i,j}^{n-1} + \omega_{i-1,j}^{n})\right.$$

$$\left.\left. + \frac{1}{(\Delta\theta)^2}(\omega_{i,j+1}^{n} - \omega_{i,j}^{n-1} + \omega_{i,j-1}^{n})\right\} - J_{i,j}\right], \qquad (20)$$

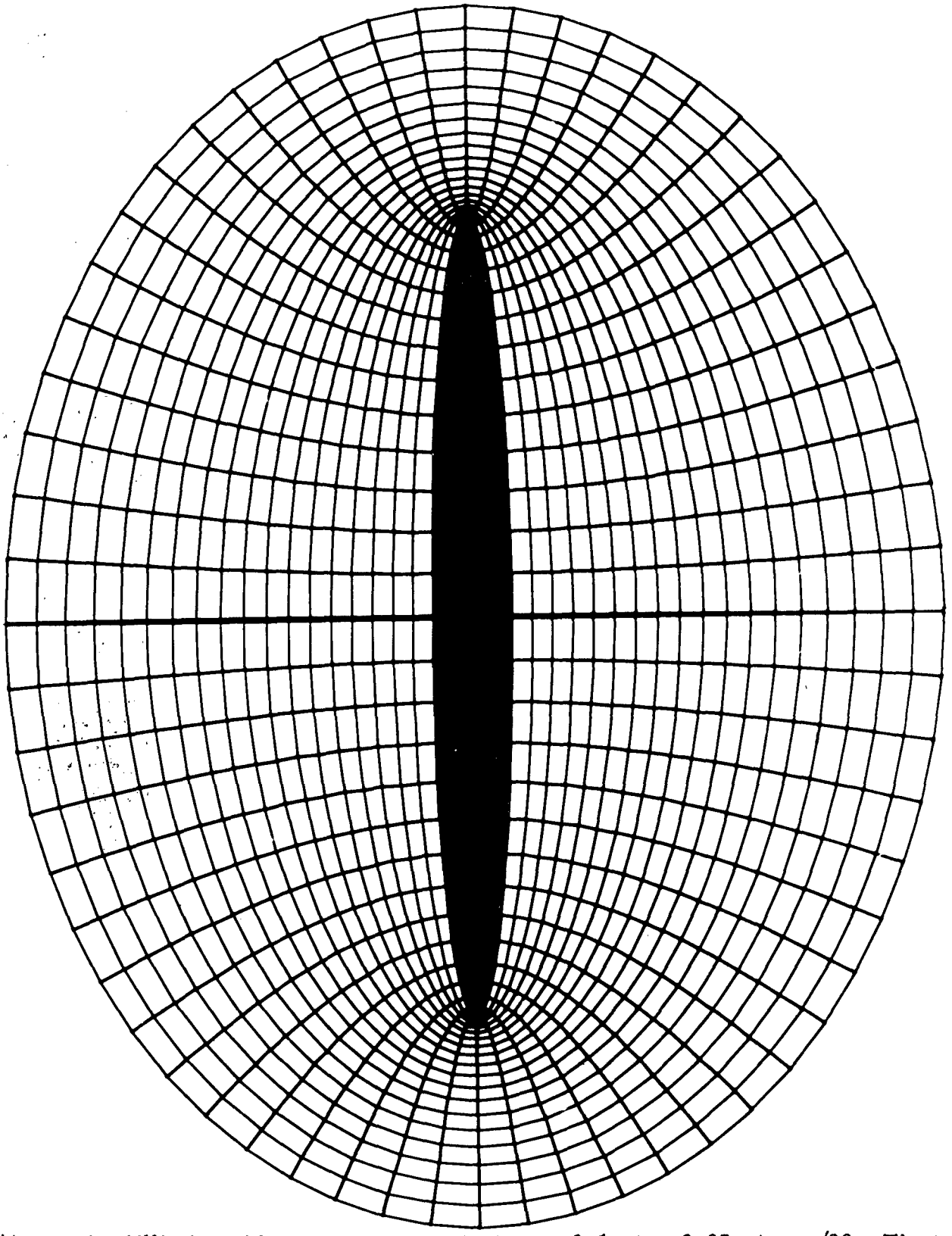

Figure 2 - Elliptic grid system near the body, $\eta_1 = 0.1$, $\Delta\eta = 0.05$, $\Delta\theta = \pi/30$. The total number of grid points is 75 x 60 = 4500

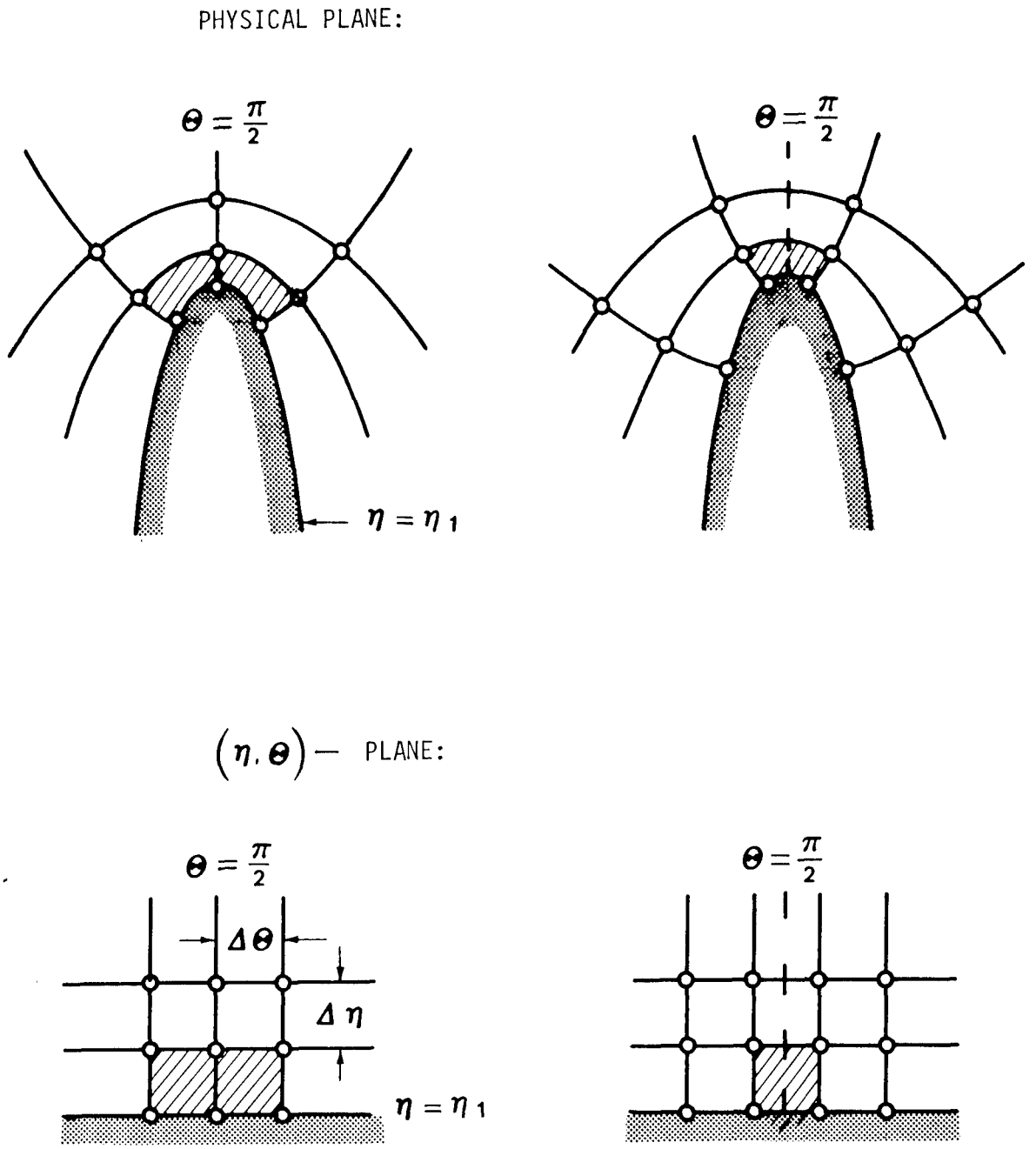

(a) the Tip is a Grid Point, (b) the Tip is Excluded from the Grid

Figure 3 - Grid near the tip. The cells closest to the tip are shaded.

where the Jacobian is

$$J_{i,j} = \frac{1}{h_{i,j}^2} \left[\frac{1}{2\Delta\eta} \left\{ (hv_\eta \omega)_{i+1,j} - (hv_\eta \omega)_{i-1,j} \right\} + \frac{1}{2\Delta\theta} \left\{ (hv_\theta \omega)_{i,j+1} - (hv_\theta \omega)_{i,j-1} \right\} \right] \tag{21}$$

and the velocity components

$$(v_\eta)_{i,j} = - \frac{1}{h_{i,j}} \frac{\psi_{i,j+1} - \psi_{i,j-1}}{2\Delta\theta}, \quad (v_\theta)_{i,j} = \frac{1}{h_{i,j}} \frac{\psi_{i+1,j} - \psi_{i-1,j}}{2\Delta\eta} . \tag{22}$$

It is recognized that central difference schemes for the Jacobian cause oscillations in ω which result in "cancer cells". These oscillations destroy the quality of the solutions for larger Reynolds numbers unless smaller space increments are employed. Hence, the capacity of the computer sets an upper limit on the Reynolds number. With the space increments $\Delta\eta = 0.05$ and $\Delta\theta = 6^\circ$ generally used in this report, the upper limit is about Re = 300 (see also Reference 18). Improvements were found by Fromm[19] and Dawson and Marcus[11] who applied fourth order approximations and a combination of central difference and backward-forward schemes, respectively. Since the present study is restricted to the pure Kármán vortex street range, with Re < 300, the simple central-difference scheme was adopted.

Equation (3) is approximated by the five-point formula which yields, for $\psi_{i,j}$,

$$\psi_{i,j} = \frac{1}{2} \frac{1}{(\Delta\eta)^2 + (\Delta\theta)^2} \Big[(\Delta\theta)^2 (\psi_{i+1,j} + \psi_{i-1,j})$$

$$+ (\Delta\eta)^2 (\psi_{i,j+1} + \psi_{i,j-1}) - (\Delta\eta\,\Delta\theta)^2 h^2_{i,j}\,\omega_{i,j} \Big] . \qquad (23)$$

This system of algebraic equations is solved with Gauss-Seidel line overrelaxation applied along lines of constant η. The overrelaxation factor is 1.82. The iteration process is halted after the kth iteration if

$$|\nabla^2 \psi^k - \omega^k| < \epsilon \qquad (24)$$

at each grid point, where ϵ is of the order of 10^{-3} in most cases. For Re = 15 and 30, $\alpha = 45^0$, ϵ of the order 10^{-4} had to be used. The number of iterations varies with the magnitude of temporal change of the flow field. For Re = 200, $\alpha = 45^0$, $\eta_1 = 0.1$ the growth of the vortices attached behind the plate requires about 60 iterations per time step, whereas vortex separation needs about 130.

During the preparation of this report several sources (Wirz[6], Briley and Walls[20], Goodson*, Buzbee et al[21]) suggested to the authors that modified Peaceman-Rachford methods and methods of cyclic block reduction would result in more efficient use of computer time than the presented method. Studies of the flow problem discussed in this paper are underway to check the proposed techniques. Results will be published later.

---

* Goodson, R., Mechanical Engineering Department, Purdue University, West Lafayette, Indiana, private communication.

At the body surface a one-sided difference scheme must be used in order to calculate the vorticity $\omega_{1,j}$. That this approximation strongly affects the numerical stability was demonstrated in a previous investigation[22]. By trial and error it was found that the formula

$$\omega_{1,j} = \frac{1}{4h_{1,j}^2(\Delta\eta)^2}\left(\psi_{2,j} + 4\psi_{3,j} - \psi_{4,j}\right) \tag{25}$$

yields the best results. This equation is derived from the Taylor series expansions with the nonslip condition $(\partial\psi/\partial\eta)_{1,j} = 0$ incorporated

$$\left(\frac{\partial\psi}{\partial\eta}\right)_{2,j} = \left(\frac{\partial^2\psi}{\partial\eta^2}\right)_{1,j}\Delta\eta + \frac{1}{2}\left(\frac{\partial^3\psi}{\partial\eta^3}\right)_{1,j}(\Delta\eta)^2 + O\left[(\Delta\eta)^3\right]$$

$$\left(\frac{\partial\psi}{\partial\eta}\right)_{3,j} = 2\left(\frac{\partial^2\psi}{\partial\eta^2}\right)_{1,j}\Delta\eta + 2\left(\frac{\partial^3\psi}{\partial\eta^3}\right)_{1,j}(\Delta\eta)^2 + O\left[(\Delta\eta)^3\right] \tag{26}$$

By using $\omega_{1,j} = \left(\frac{1}{h^2}\frac{\partial^2\psi}{\partial\eta^2}\right)_{1,j}$ and replacing $\left(\frac{\partial\psi}{\partial\eta}\right)_{i,j}$ with

$$\frac{1}{2\Delta\eta}\left(\psi_{i+1,j} - \psi_{i-1,j}\right) + O\left[(\Delta\eta)^2\right] \tag{27}$$

one arrives at Equation (25). Hence, Taylor series expansions are used which result in an expression for $\omega_{1,j}$ with error of second order in $\Delta\eta$. However, when first derivatives at inner points are replaced by finite differences, the final formula for $\omega_{1,j}$ is of the first order. The hybrid form, Equation (25), is more stable than the first order approximation used by most other investigators

$$\omega_{1,j} = \frac{2\psi_{2,j}}{h_{1,j}^2(\Delta\eta)^2} + O(\Delta\eta) \tag{28}$$

and much more stable than second order approximations investigated, for instance,

$$\omega_{1,j} = \frac{1}{2h_{1,j}^2(\Delta\eta)^2}(8\psi_{2,j} - \psi_{3,j}) + O\left[(\Delta\eta)^2\right] . \tag{29}$$

In fact, it was found that Δt_{max} is about 10 times smaller for Equation (28) and 100 times smaller for Equation (29) than Δt_{max} for Equation (25). However, the statement that Equation (25) is superior to Equation (28) is not valid in general. For instance, in other work[23] we found Equations (25) and (28) to be comparable with regard to stability.

Since the domain of numerical integration is bounded, severe difficulties are encountered in prescribing the conditions at the outer boundary $\eta = \eta_L$. This boundary is almost circular and is divided in half. On the upstream half of the boundary, the conditions (6) are used with the alteration that the second condition is replaced by vanishing vorticity:

$$\eta = \eta_L , \quad \left.\begin{array}{r} 0 \le \theta \le \frac{\pi}{2} + \alpha \\ \frac{3}{2}\pi + \alpha \le \theta < 2\pi \end{array}\right\} : \frac{\partial\psi}{\partial\eta} = h \sin(\theta - \alpha), \ \omega = 0 . \tag{30}$$

In difference form (tip point not included in grid):

$$\left(\frac{\partial\psi}{\partial\eta}\right)_{L,j} = h_{L,j} \sin\left[(j - \frac{1}{2})\Delta\theta - \alpha\right], \quad \omega_{L,j} = 0 . \tag{31}$$

On the downstream half of the boundary a convection type condition is used:

$$\eta = \eta_L , \quad \frac{\pi}{2} + \alpha < \theta < \frac{3}{2}\pi + \alpha :$$

$$\frac{\partial \omega}{\partial t} + \frac{1}{U} (\vec{U} \cdot \nabla) \omega = 0 ,$$

$$\left[\frac{\partial \vec{v}}{\partial t} + \frac{1}{U} (\vec{U} \cdot \nabla) \vec{v} \right]_\theta = 0 . \tag{32}$$

This type of condition was proposed by Dawson and Marcus[11] for the vorticity and seems to work well when extended as above to the velocity. With the difference approximations of Equations (32) the values of ω and $\partial\psi/\partial\eta$ are computed on the boundary $\eta = \eta_L$:

$$\omega_{L,j}^{n+1} = \omega_{L,j}^{n} + \frac{\Delta t}{h_{L,j}^2} \Bigg[(\cos\alpha \sinh\eta_L \cos\theta_j + \sin\alpha \cosh\eta_L \sin\theta_j) \left(\frac{\omega_{L,j}^{n} - \omega_{L-1,j}^{n}}{\Delta\eta} \right) + (\sin\alpha \sinh\eta_L \cos\theta_j - \cos\alpha \cosh\eta_L \sin\theta_j) \left(\frac{\omega_{L,j+1}^{n} - \omega_{L,j-1}^{n}}{2\,\Delta\theta} \right) \Bigg] , \tag{33}$$

$$\left(\frac{\partial\psi}{\partial\eta}\right)^{n+1}_{L,j} = \left(\frac{\partial\psi}{\partial\eta}\right)^{n}_{L,j} + \frac{\Delta t}{2\Delta\theta}\Bigg[(\cos\alpha\sinh\eta_L\cos\theta_{j+1} + \sin\alpha\cosh\eta_L\sin\theta_{j+1})$$

$$\cdot\frac{v^{n}_{\eta_{L,j+1}}}{h_{L,j+1}} - (\cos\alpha\sinh\eta_L\cos\theta_{j-1} + \sin\alpha\cosh\eta_L$$

$$\sin\theta_{j-1})\frac{v^{n}_{\eta_{L,j-1}}}{h_{L,j-1}}$$

$$+ (\sin\alpha\sinh\eta_L\cos\theta_{j+1} - \cos\alpha\cosh\eta_L\sin\theta_{j+1})\frac{v_{\theta L,j+1}}{h_{L,j+1}}$$

$$- (\sin\alpha\sinh\eta_L\cos\theta_{j-1} - \cos\alpha\cosh\eta_L\sin\theta_{j-1})\frac{v_{\theta,j-1}}{h_{L,j-1}}$$

$$+ 2\Delta\theta(\cos\alpha\sinh\eta_L\cos\theta_j + \sin\alpha\cosh\eta_L\sin\theta_j)\omega^{n}_{L,j}\Bigg] . \qquad (34)$$

The decision to use convection equations of the type in Equations (32) is heuristic and guided by the idea of interfering with the downstream flow as little as possible. Photographs of wind-tunnel flows reveal that the shapes of the vortices are well preserved over many cycles of the Kármán vortex street.

The integration process is carried out in the following way: The vorticity $\omega^{n+1}_{i,j}$ for the advanced time step (n+1) is computed at the inner points according to Equation (20). Next, $\omega^{n+1}_{L,j}$ and $(\partial\psi/\partial\eta)^{n+1}_{L,j}$ are determined on the downstream boundary points by means of

Equations (33) and (34). Then $\psi_{i,j}^{n+1}$ is calculated with the aid of Equation (23). The cycle concludes with the calculation of $\omega_{1,j}^{n+1}$ from Equation (25).

The maximum stable time step Δt_{max}, beyond which numerical instability occurs, is determined by increasing the time step until oscillations from one time step to another appear in the ω-values near the tips. The magnitude of Δt_{max} depends on factors other than ω_1. It is a linear function of the Reynolds number, at least for Re $\leq$ 200, and decreases rapidly as either $\Delta\eta$, $\Delta\theta$, or η_1 approaches zero[18]. There seems to be no dependence on α. Computer time is saved by enlarging η_1 as much as possible without the loss of the essential features of the flat plate (if η_1 is changed from 0.05 to 0.1, Δt_{max} increases fourfold). The values of Δt_{max} are for $\eta_1 = 0.1$, tip point out,

Re	α	Δt_{max}
15	45°	0.0004
30	45°	0.0007
50	90°	0.0012
200	0°, 45°	0.005

Smaller time steps are necessary near t = 0, when large vorticity gradients are present. For high surface curvature, that is for $\eta_1 < 0.1$, stability is improved if the grid system is shifted by $\Delta\theta/2$ in the θ-direction so that there are no grid points at the tips. This does not affect the overall accuracy of the solution and, in addition to improving the stability, makes possible the computation of the flow field when $\eta_1 = 0$[17].

Accuracy considerations are similar to those for the flow past oblate spheroids[18]. Additional information on the quality of the solution is obtained by integrating $\partial\omega/\partial\eta$ over the body contour. The integral of this function over a segment of the surface is the pressure difference between the end points of the segment. Hence, the integration around the entire contour of the body should yield zero and is a sensitive test which must be passed to a certain degree by any accurate solution. For Re = 200, $\alpha = 45^{\circ}$, $\eta_1 = 0.1$, the value of this integral is always smaller than 3% of the difference between the maximum and minimum pressure at the surface. Other "confidence-building" tests compare our results to those obtained with different methods.

The numerical calculation of the drag, lift, and moment coefficients is sensitive to the difference scheme used for the approximation of the integrals of Equations (11) through (19)[17]. These coefficients can be computed either with the aid of a double integral (for C_{DP} it is formula (11)) or by means of a single integration (for C_{DP} it is formula (13)). For both methods two difference schemes have been checked and are presented here for the example $\int_0^{2\pi} p_1 \cos\theta \, d\theta$ with the tip not included in the grid:

Simpson's rule:

$$\int_0^{2\pi} p_1 \cos\theta \, d\theta = \frac{\Delta\theta}{3}\left[2 p_{1,1} \cos\frac{\Delta\theta}{2} + 4 p_{1,2} \cos\left(\frac{3}{2}\Delta\theta\right) + 2 p_{1,3} \cos\left(\frac{5}{2}\Delta\theta\right) + \ldots + 4 p_{1,M} \cos\left(\frac{2M-1}{2}\Delta\theta\right)\right] \quad (35)$$

Second approximation:

$$\int_0^{2\pi} p_1 \cos\theta \, d\theta = \sum_{j=1}^{M} \Delta\theta \, p_{1,j} \cos\left\{(j - \tfrac{1}{2})\Delta\theta\right\} . \tag{36}$$

For the grid which does not contain the tip point the following values have been computed: Re = 50, $\alpha = 90^{\circ}$, $\eta_1 = 0.1$, t = 1.71.

	C_{DP}	C_{DF}
Double integration:		
Simpson's rule:	5.67	0.230
Approximation (36):	5.67	0.230
Single integration:		
Simpson's rule:	6.50	0.230
Approximation (36):	5.67	0.230

If the tip point is included in the grid, the data for the case Re = 50, $\alpha = 90^{\circ}$, $\eta_1 = 0.05$, t = 2.31 are

Double integration:		
Simpson's rule:	5.21	0.097
Single integration:		
Simpson's rule:	2.70	0.097
Approximation (36):	5.20	0.105

Based on earlier results[17] where theory and experiment were compared, it is assumed that the worst result is obtained with the single integration by using Simpson's rule. Unfortunately, this case was reported in the condensed version of this paper, Lecture Notes in Physics 8, 1971, Springer Verlag, p. 78. The value of 2.8 given in this paper for Re = 50, $\alpha = 90^{\circ}$, $\eta_1 = 0.05$, t = 2.13 is not correct. Throughout the present report the single integration by using approximation (36) is employed.

RESULTS

All computations were carried out in double precision on an IBM 360-91 computer. The graphic display of streamlines and lines of constant vorticity was produced with a Stromberg-Carlson SC-4020 charactron plotter. The examples selected for computation are compiled in Table 1.

Symmetric Flows

For the symmetric flow configurations, which according to experiments are expected for $\alpha = 0^{\circ}$, $Re < 200$, $\eta_1 \leq 0.1$ and $\alpha = 90^{\circ}$, $Re < 50$, η_1 arbitrary, a steady state is approached as $t \to \infty$. For $Re = 10$, $\alpha = 90^{\circ}$, $\eta_1 = 0.1$ one aspect of the transient stage is displayed in Figure 4, where the drag coefficient is plotted against time. Figures 5 and 6 show the streamlines and lines of constant vorticity for the almost steady state $t = 11.2$. The development of the twin vortices behind the body is recorded in Figure 7, where the dimensionless length of the wake s/d is plotted against time. Although the steady-state value measured by Taneda[24] is approached quite accurately, the data for the transient stage are low compared with the empirical formula developed by Taneda and Honji[25]

$$s/d = 0.89\,(t/2)^{2/3}, \quad Re \geq 18.1 \tag{37}$$

This relation, which does not contain the kinematic viscosity ν, holds only for an intermediate time interval. As can be seen immediately from Figure 7, the wake length approaches a finite value when $t \to \infty$, a process which is governed by viscous forces. Near $t = 0$, Equation (37) cannot be valid either. As shown also in Taneda and Honji's experiments[25],

TABLE 1 - COMPILATION OF THE CALCULATED EXAMPLES

Re_d	α	η_1	t_{FINAL}	GRID	TIP IS GRID POINT
10	90°	0.1	11.2	75 x 60	NO
15	45°	0.1	7.2	75 x 60	NO
30	45°	0.1	16.3	75 x 60	NO
50	0°	0.1	1.5	75 x 60	YES
50	90°	0.05	2.3	75 x 60	YES
50	90°	0.1	3.5	75 x 60	NO
200	0°	0.1	18.7	75 x 60	YES
200	10°	0	1.9	75 x 80	NO
200	45°	0	0.04	75 x 80	NO
200	45°	0.1	30.0	75 x 60	NO
200	45°	0.2	8.1	75 x 60	NO
200	45°	0.2	11.5	75 x 80	NO

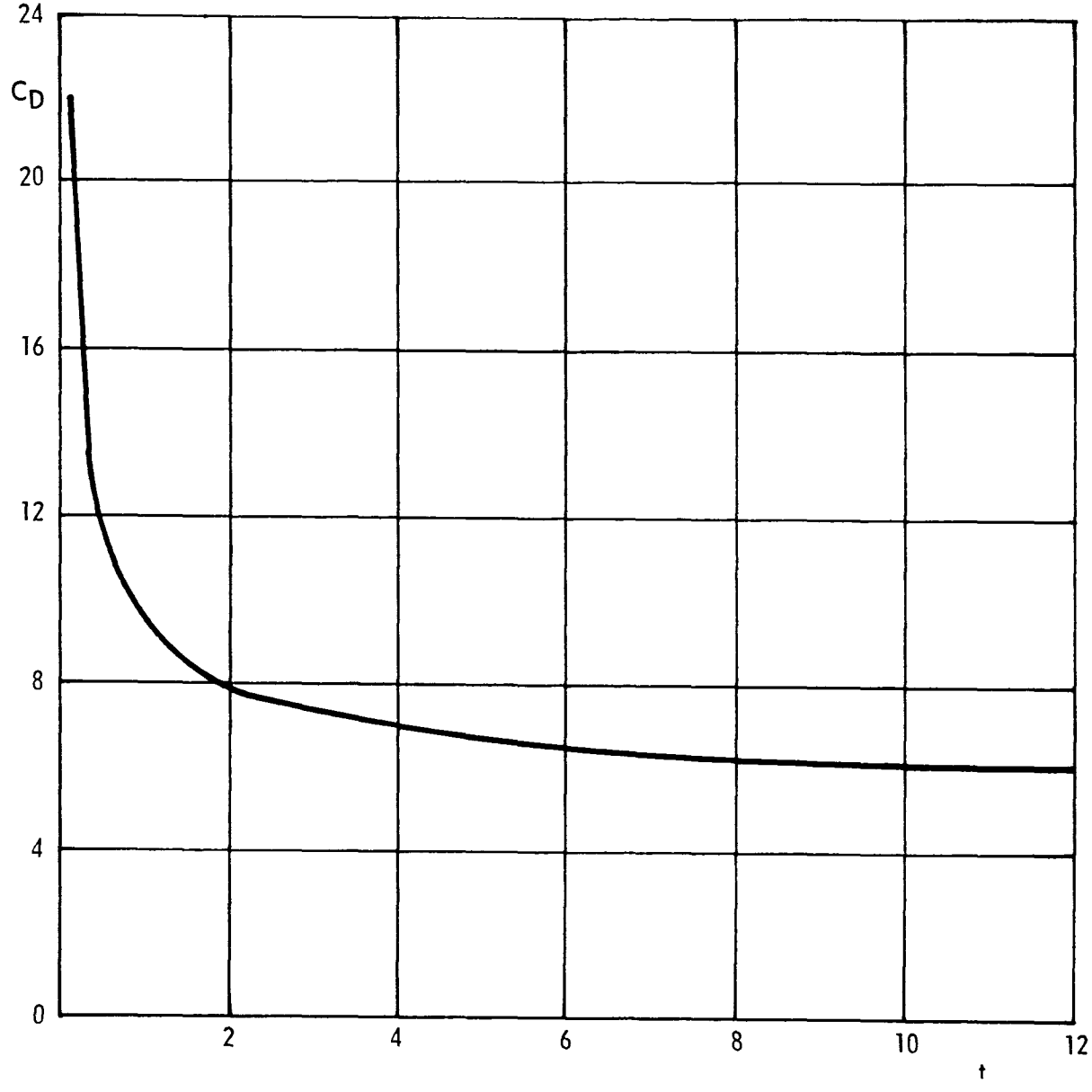

Figure 4 - Drag coefficient versus time for Re = 10, $\alpha = 90^{\circ}$, $\eta_1 = 0.1$

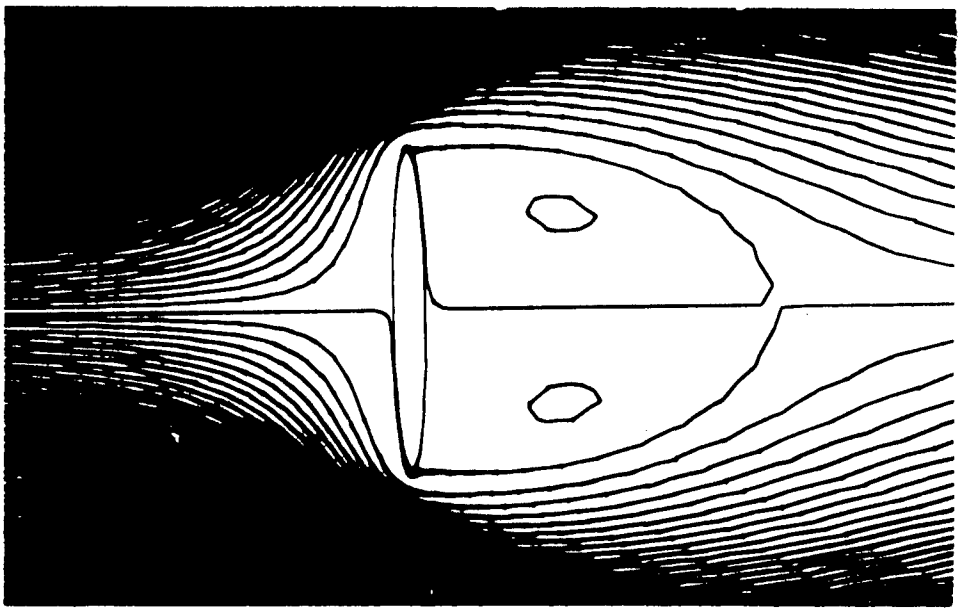

Figure 5 - Streamlines for Re = 10, $\alpha = 90^{\circ}$, $\eta_1 = 0.1$ at t = 11.2 (almost steady state)

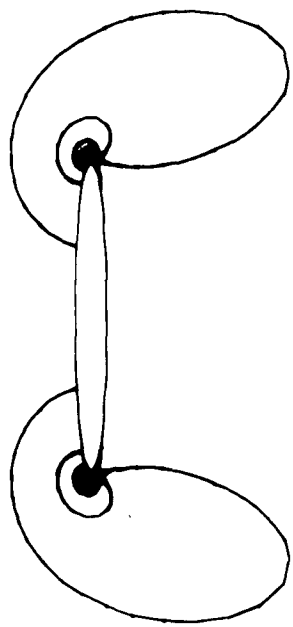

Figure 6 - Lines of constant vorticity for Re = 10, $\alpha = 90^{\circ}$, $\eta_1 = 0.1$ at $t = 11.2$ (almost steady state)

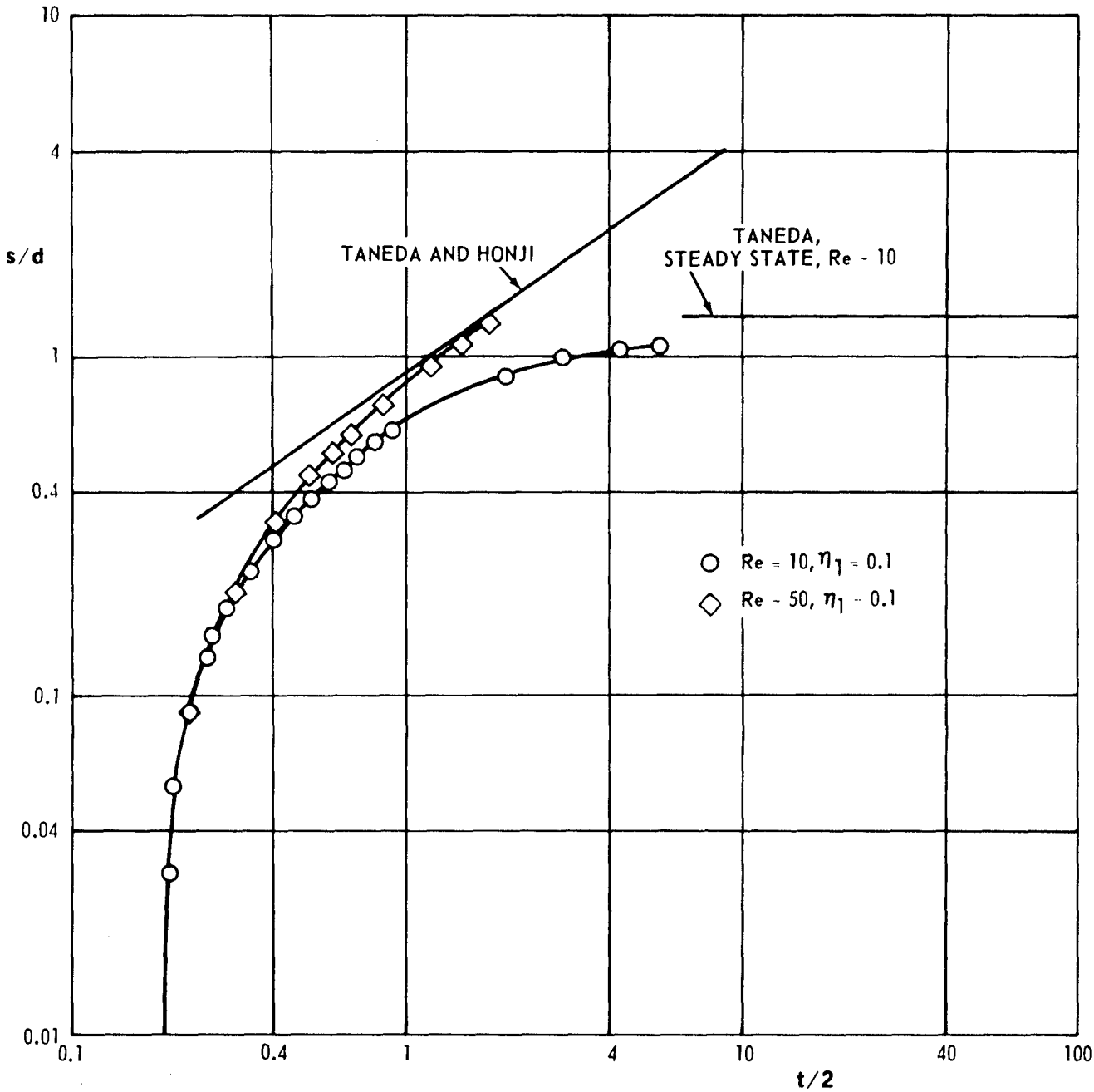

Figure 7 - Dimensionless wake length versus time for Re = 10 and 50, $\alpha = 90^{\circ}$, $\eta_1 = 0.1$

the vortices are generated at the tips and then join at the centerline after a certain time (Figure 8). The instant at which they join is the beginning of the wake development with nonvanishing s. For small Reynolds numbers the two time periods which are excluded from Equation (37) overlap and the curve of Equation (37) is not reached. This appears to be the reason for the low values at Re = 10.

The drag coefficients for the almost steady state are compared with other sources in Table 2.

TABLE 2 - DRAG COEFFICIENTS FOR SYMMETRIC FLOW CONFIGURATIONS

α	Re	η_1	t_{FINAL}	C_D	
				Computed	From Dennis & Chang[4]
0°	50	0.1	1.50	1.39	1.432 (for Re = 40)
0°	200	0.1	18.7	0.55	0.492 (for $\eta_1 = 0$)
90°	10	0.1	11.2	6.02	----

The values for $\alpha = 0^o$ compare favorably with the steady-state solutions of Dennis and Chang[4].

It may be mentioned that in the condensed version of this paper, published in the Lecture Notes in Physics, No. 8, Springer-Verlag, 1971, the case $\alpha = 90^o$, Re = 50, $\eta_1 = 0.05$, t = 2.13 was considered as an almost steady state. This statement is incorrect, since the wake grows considerably larger when $t \to \infty$.[24]

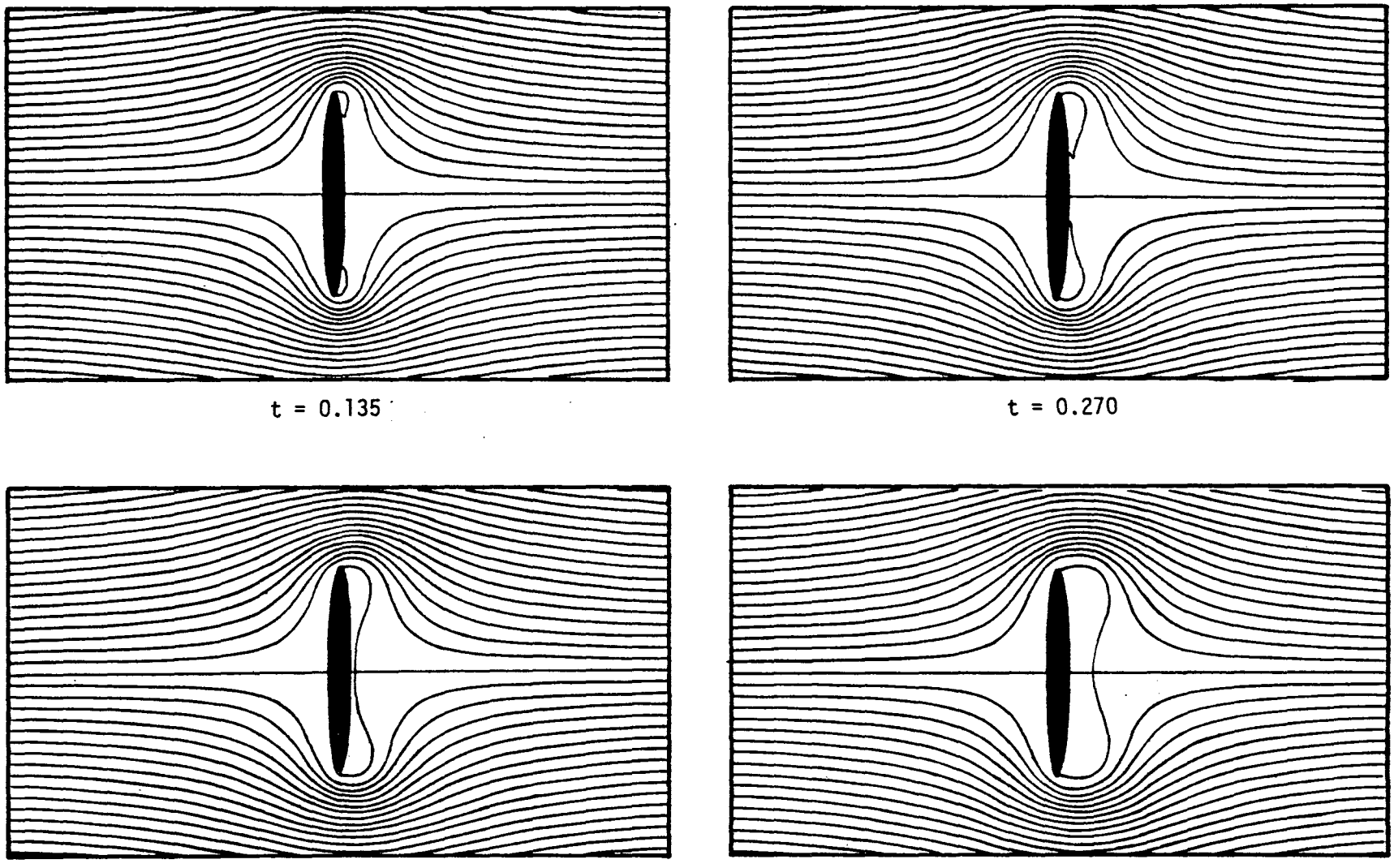

Figure 8 - Sequence of streamlines in the initial phase of wake development for Re = 50, $\alpha = 90^{\circ}$, $\eta_1 = 0.1$

Nonsymmetric Flows

Most of the numerical data compiled are obtained for the nonsymmetric case $\alpha = 45^{\circ}$, Re = 200. The first series of pictures, which is shown in Figure 9, is selected to display the flow behavior following the abrupt start of the body at t = 0. Immediately after t = 0, in the initial potential-flow field, a starting vortex forms and separates from the trailing edge. In the streamline pictures this vortex is visible as a wavy pattern which indicates the movement of the vortex relative to the plate (which is kept at rest). The lines of constant vorticity clearly exhibit a local extremum at the center of the vortex. In the early time period the zero streamline migrates from the rear stagnation point of the potential flow to the trailing edge. This verifies, even for the low Reynolds number Re = 200, the hypothesis of Lanchester-Prandtl, that circulation around an airfoil is generated by a starting vortex and that the zero streamline follows a kind of Kutta condition.

The computation of the case Re = 200, $\alpha = 45^{\circ}$, $\eta_1 = 0.1$ was carried out over three cycles of vortex shedding. The last cycle was repeated with the fine mesh $\Delta\eta = 0.05$, $\Delta\theta = \pi/40$. The flow patterns of the third cycle obtained with the fine mesh are displayed in Figure 10. The development and the detachment of the vortices are similar to those of the first cycle in Figure 9. An overall view of the wake is presented in Figure 11. To the right the boundary of the grid system is visible. The location of the vortices shows that the vortex street is not parallel to the undisturbed flow.

In Figure 12 the drag, lift, and torque coefficients are plotted against time t. The abrupt start of the body requires infinite values for C_D and C_L, whereas the C_M-value begins from zero. The Strouhal

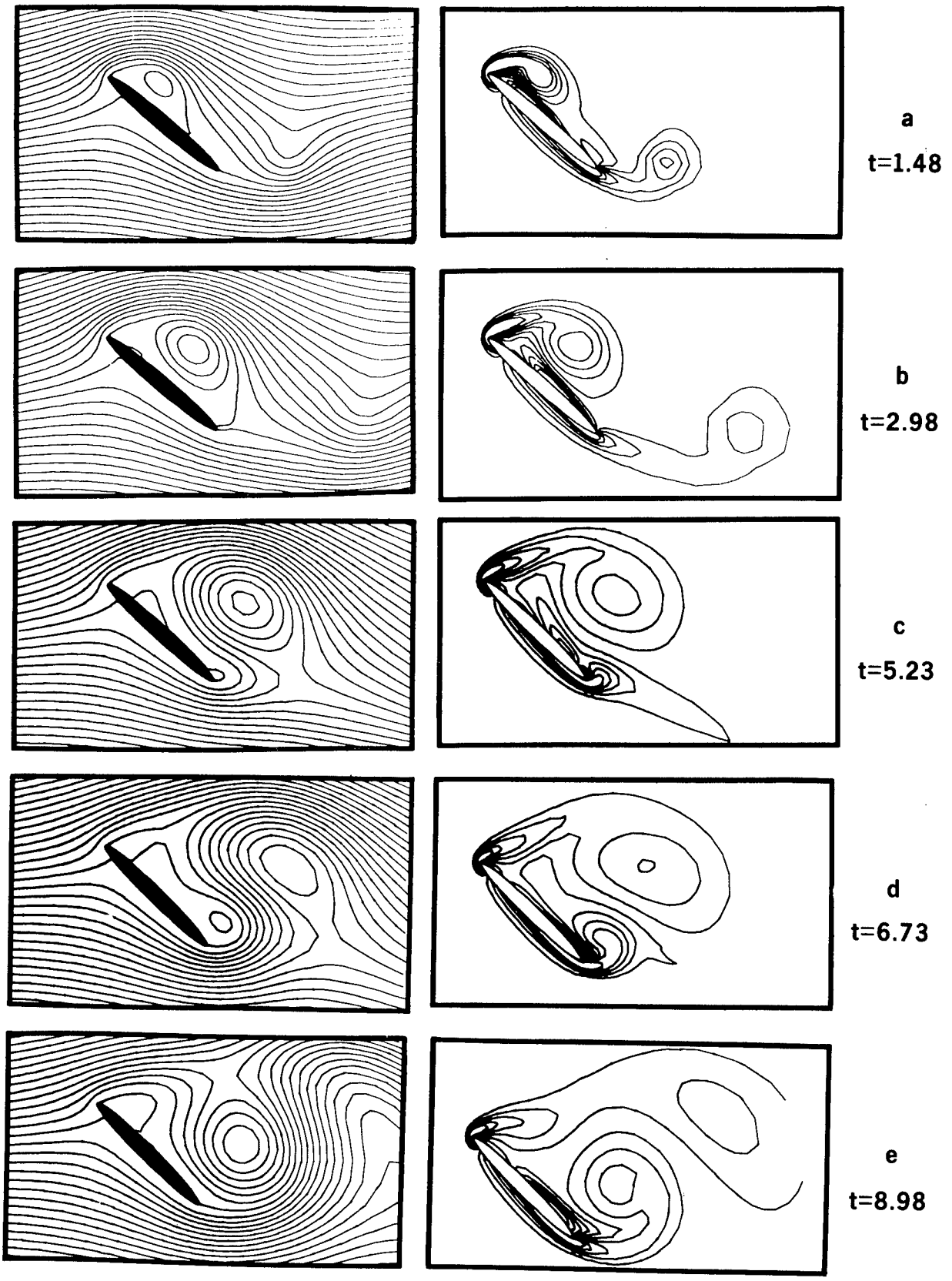

Figure 9 - Sequence of streamlines and equal-vorticity lines for Re = 200, $\alpha = 45^{o}$, $\eta_1 = 0.1$ at various times after the abrupt start. Potential flow at t = 0

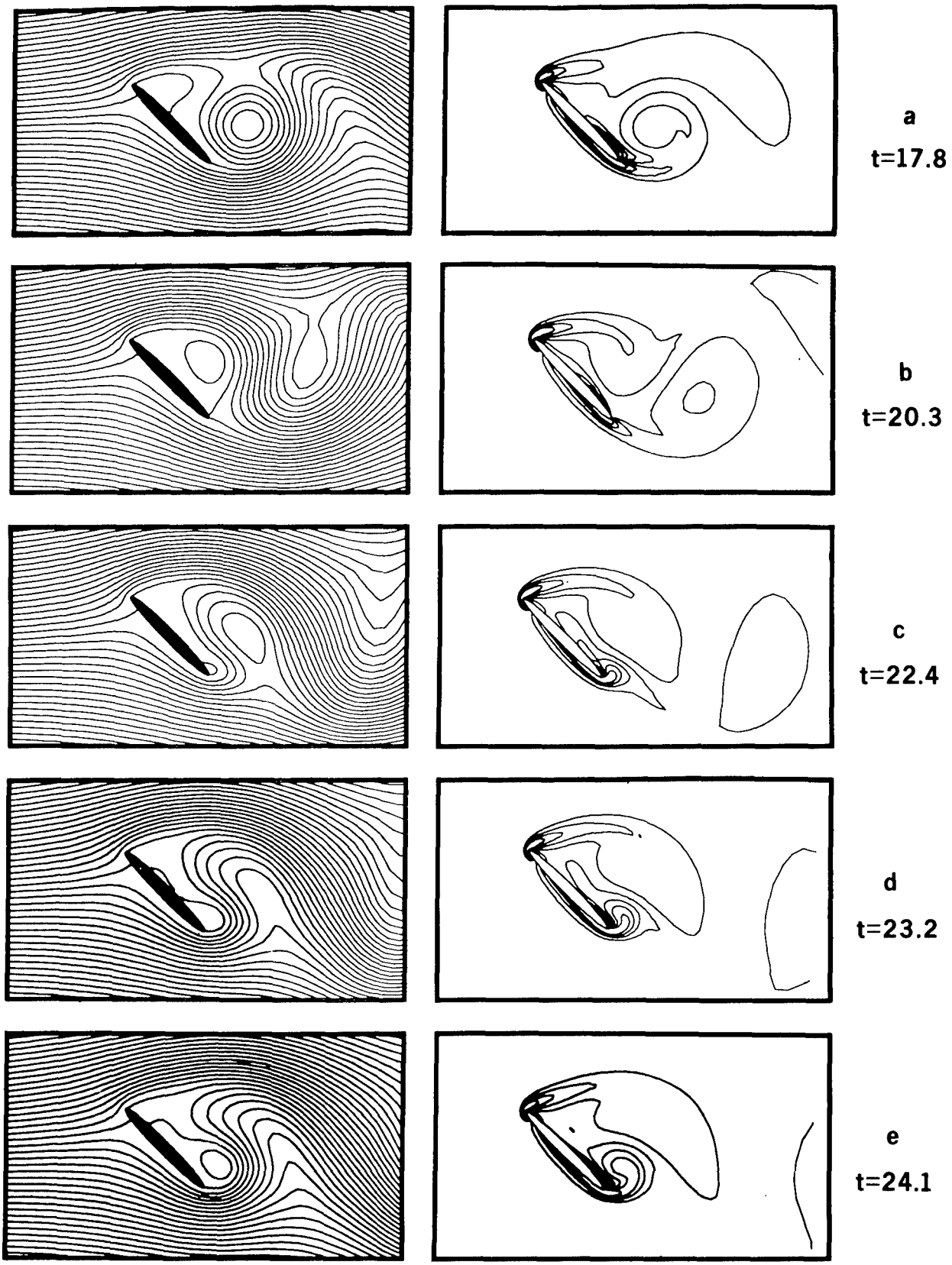

Figure 10 - Sequence of streamlines and equal-vorticity lines for the third cycle of Re = 200, $\alpha = 45^{\circ}$, $\eta_1 = 0.1$ after the abrupt start

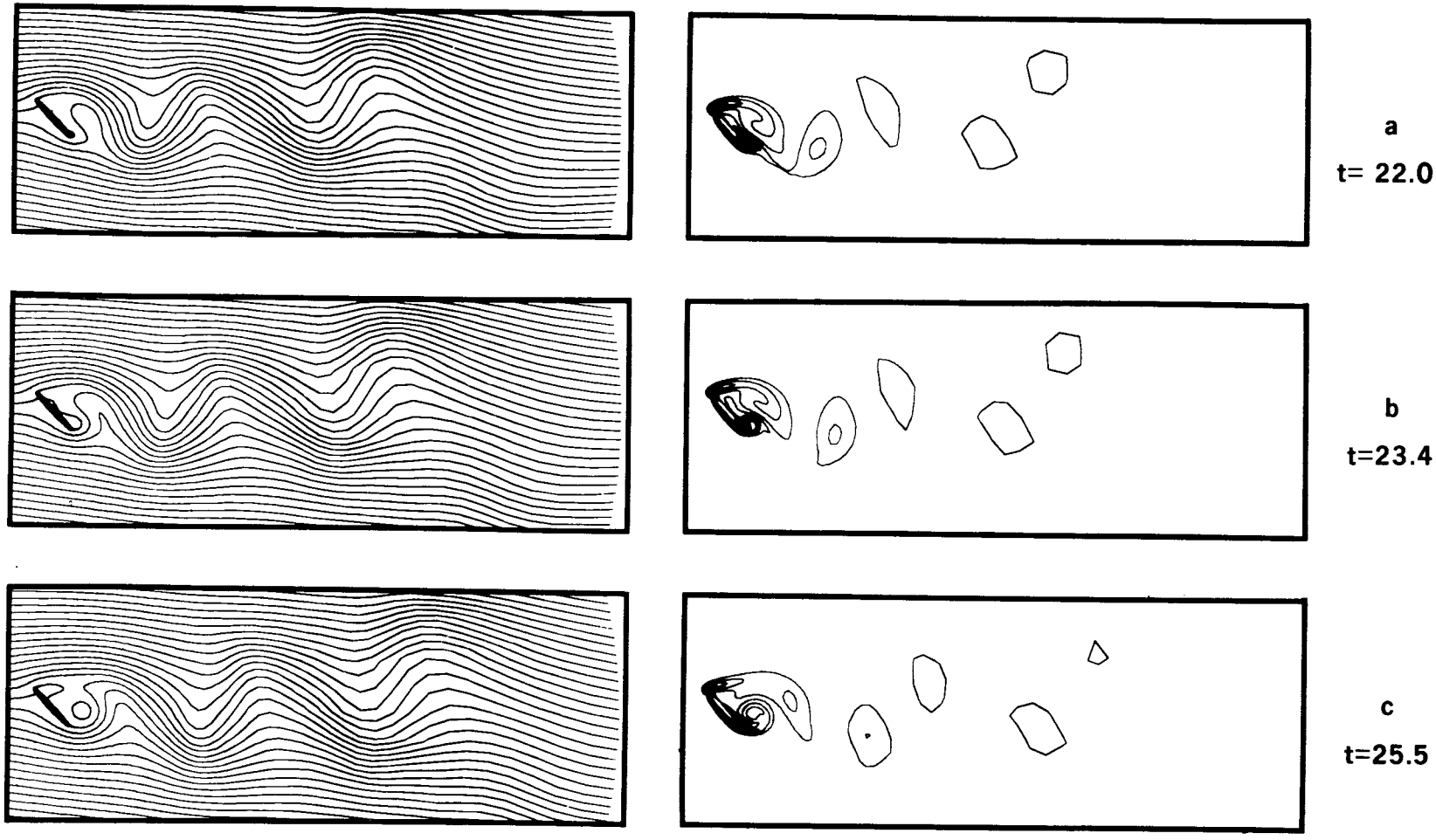

Figure 11 - Some patterns of streamlines and equal-vorticity lines of the entire wake region for Re = 200, $\alpha = 45^{o}$, $\eta_1 = 0.1$ during the third cycle

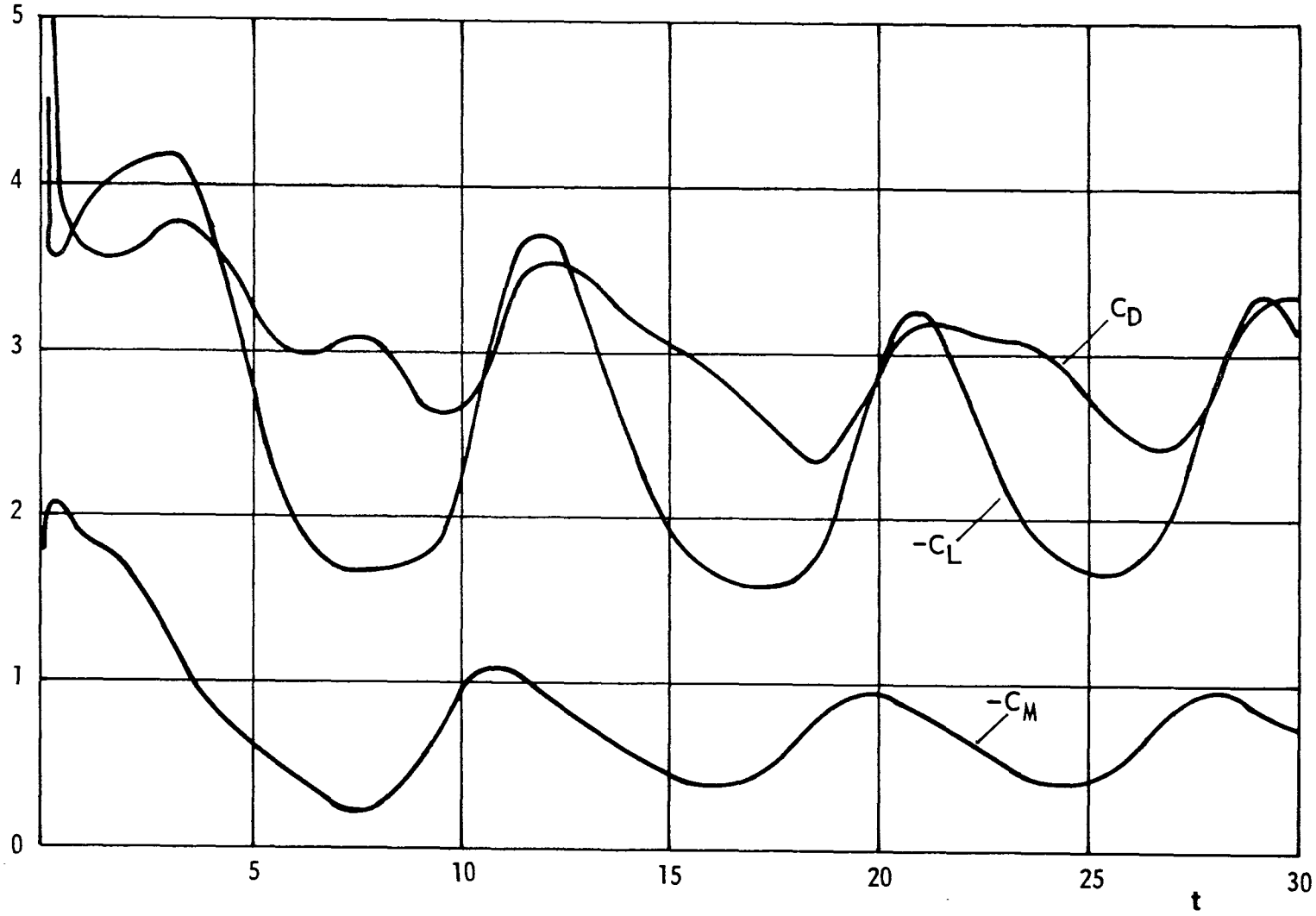

Figure 12 - Drag, lift, and moment coefficients versus time for Re = 200, $\alpha = 45^{\circ}$, $\eta_1 = 0.1$

number which is defined by

$$St = \frac{dn}{U} \tag{38}$$

is about 0.23 for the second cycle and 0.25 for the third. In Equation (38) n is the frequency of the vortex shedding. If one relates the Strouhal number to the projected plate width $d \sin \alpha$, the values for the second and third cycles are 0.163 and 0.177, respectively.

A comparison of Figures 10 and 12 reveals that the coefficients C_D, C_L, and C_M assume relative maxima whenever a vortex separates from the leading edge.

In Figure 13 the coefficients C_{DF} and C_{LF} are plotted against time for Re = 200, $\alpha = 45^{\circ}$, $\eta_1 = 0.1$.

For $\eta_1 = 0.2$ computations have been made with $\Delta\theta = \pi/30$ as well as with $\Delta\theta = \pi/40$. The differences in the C_D, C_L, and C_M values between the two cases are so small that they cannot be observed on a graphic display.

In Figures 14 and 15 the surface vorticity and the surface pressure are plotted against θ for the third cycle of the case Re = 200, $\alpha = 45^{\circ}$, $\eta_1 = 0.1$ computed with the fine mesh. The production of vorticity at the edges is smallest when a vortex separates from the edge, and it is highest when a vortex starts growing.

Based on Timme's experiments[26] the decay of vortices in the Kármán-vortex street can be described by the Hamel-Oseen solution for each vortex:

$$v'_{\phi} = \frac{\text{const}}{r}\left(1 - e^{-(r^2/4\nu(t'-t'_0))}\right), \quad v'_r \equiv 0 \tag{39}$$

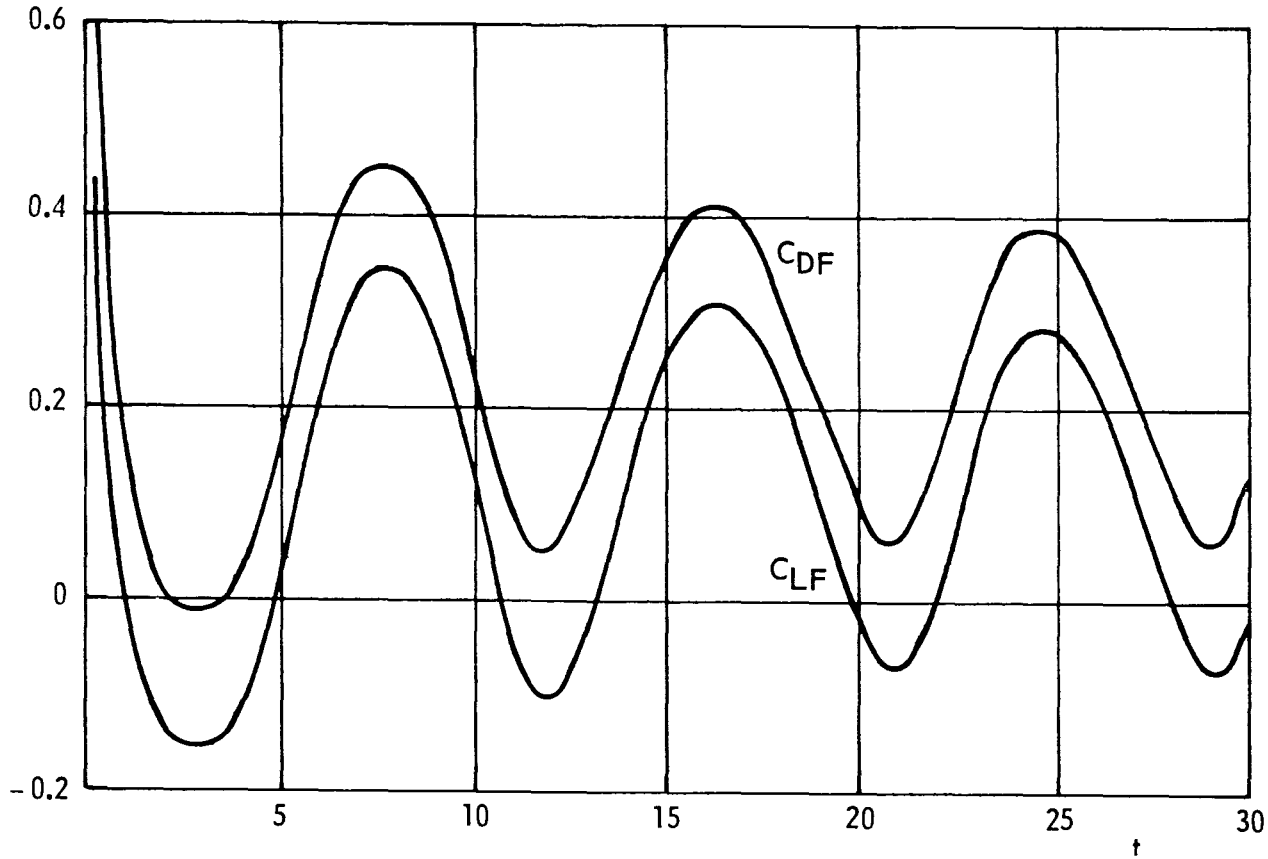

Figure 13 - Coefficients for frictional drag and lift versus time for Re = 200, $\alpha = 45^{\circ}$, $\eta_1 = 0.1$

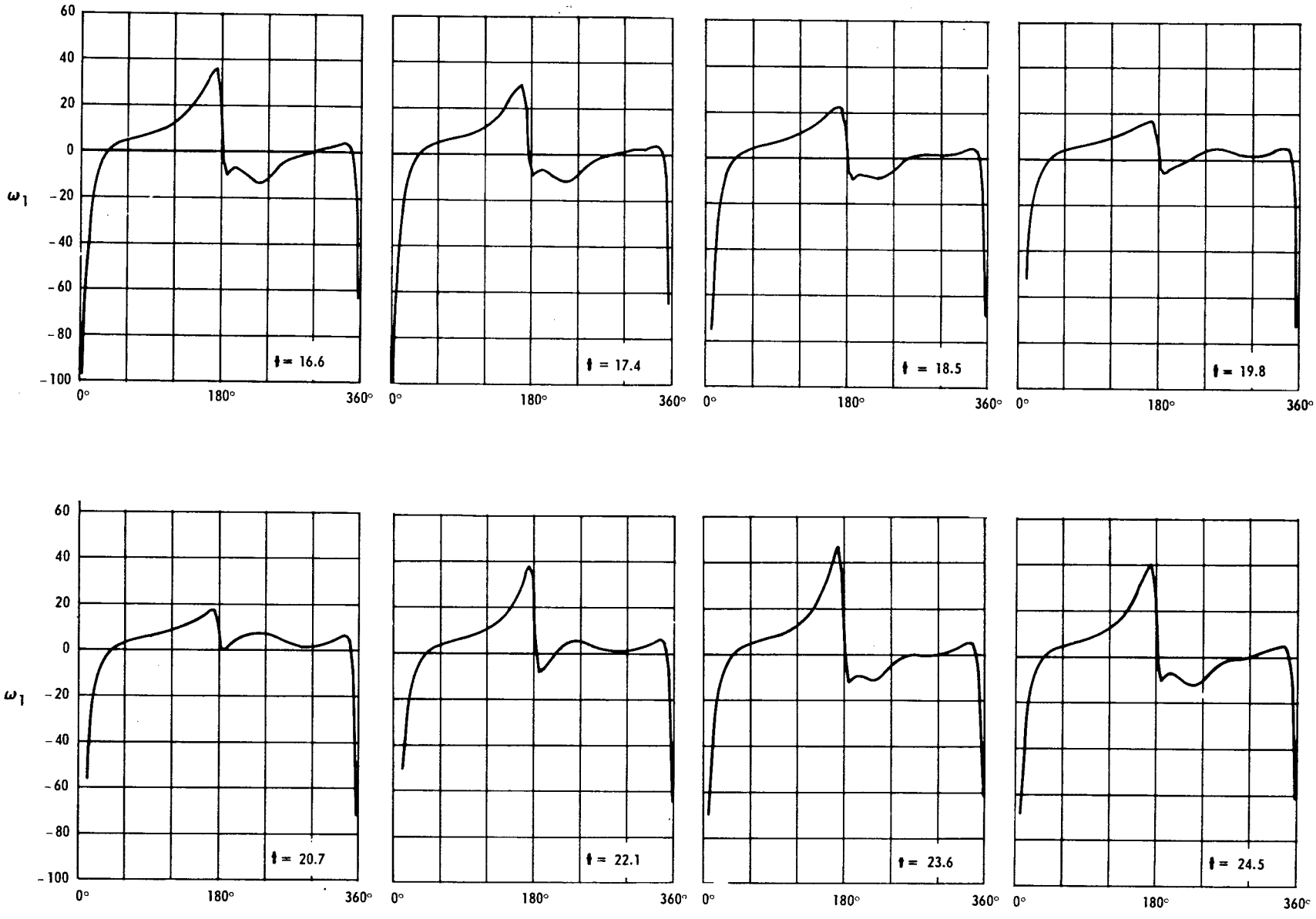

Figure 14 - Surface vorticity versus θ for the third cycle of Re = 200, $\alpha = 45^{\circ}$, $\eta_1 = 0.1$

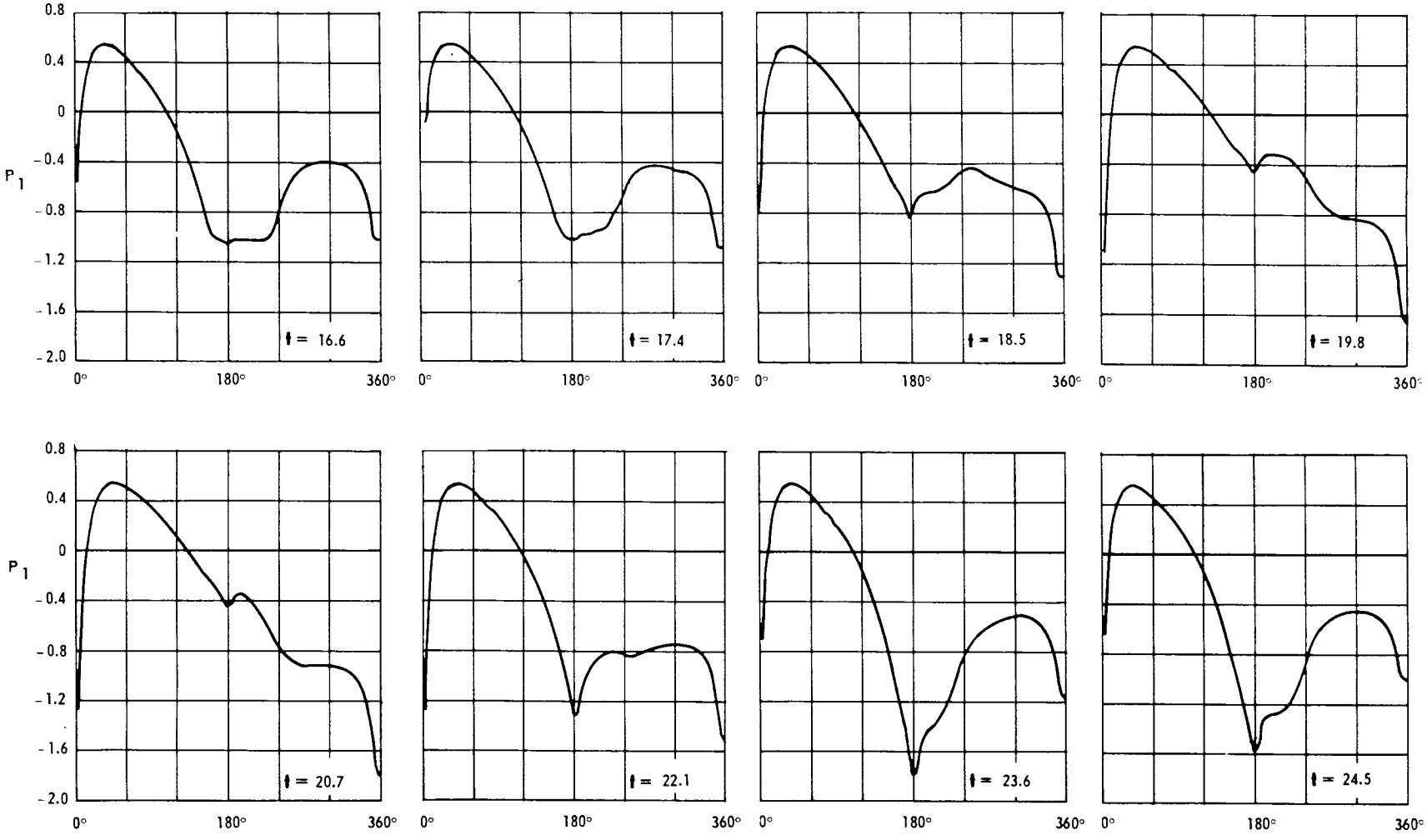

Figure 15 - Surface pressure versus θ for the third cycle of Re = 200, $\alpha = 45^{\circ}$, $\eta_1 = 0.1$

where the polar coordinates (r, ϕ) with the corresponding velocity components (v_r', v_ϕ') are used. Equation (39) represents the decay of a potential vortex from the time $t' = t_0'$. This expression represents the lowest mode of plane disturbances.[27] The vorticity at the vortex center (where the extremum of vorticity is located) dissipates according to

$$\omega'_{r=0} = \frac{\text{const}}{2\nu(t'-t_0')} \quad . \tag{40}$$

For the next higher mode of the spectrum of disturbances the vorticity $\omega'_{r=0}$ would decay as $(t'-t_0')^{-2}$, as was shown elsewhere[27]. The numerical data can be checked against the analytic prediction. In Figure 16 the decay of the central vorticity of the initial vortex for $Re = 200$, $\alpha = 45^\circ$, $\eta_1 = 0.1$ is displayed with logarithmic scales. The best fit to a linear relation between the logarithms of the central vorticity and time is obtained when $t_0 = -0.3$ and the slope is -1. Vortices which are generated after the initial vortex behave similarly. Near the outer boundary of the grid, where the mesh size increases rapidly, the numerical values deviate from the analytic curve. This deviation depends on the mesh size (see Figure 16). Apparently, the numerical solution is not accurate enough to describe the vortex decay in that part of the grid.

For $Re = 200$, some information was obtained when $\alpha = 10^\circ$, $\eta_1 = 0$. The initial phase up to $t = 1.94$ is recorded in Figures 17 and 18. Non-periodic vortex shedding from the leading edge, which has been observed*

---

* Laitone, E.V., University of California, Berkeley, private communication.

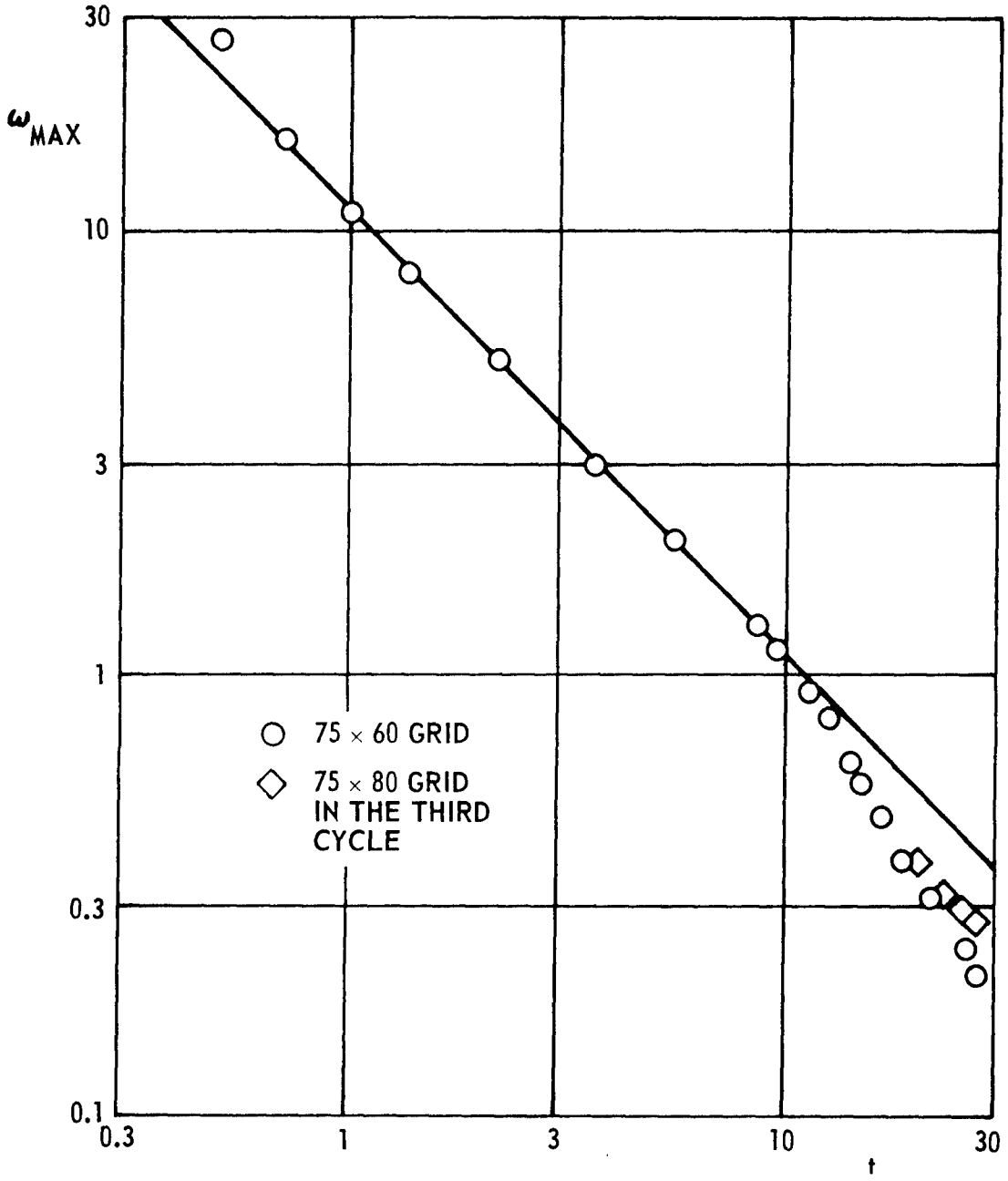

Figure 16 - Decay of central vorticity of the initial vortex for Re = 200, $\alpha = 45^{o}$, $\eta_1 = 0.1$

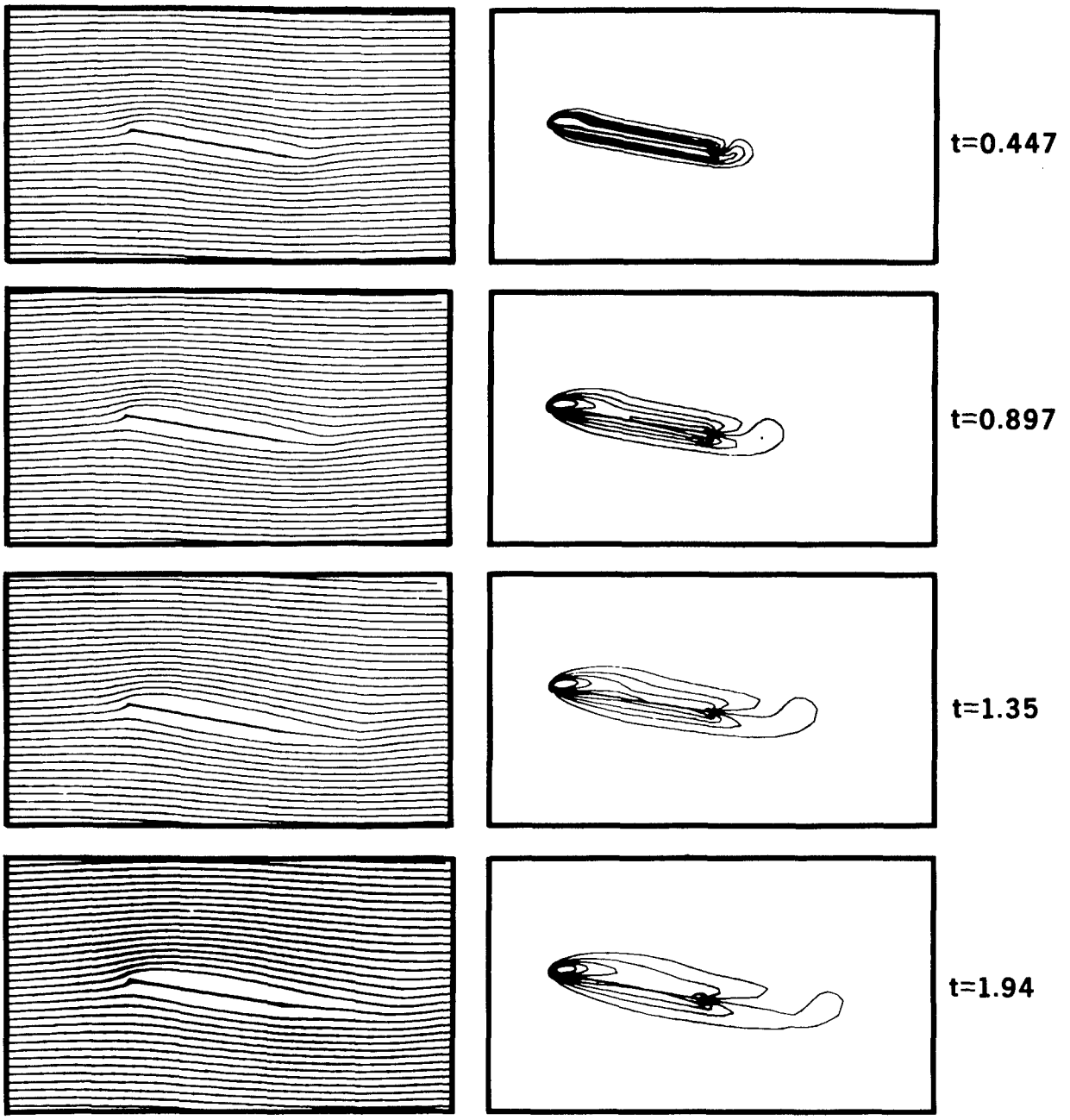

Figure 17 - Some patterns of streamlines and equal-vorticity lines for Re = 200, $\alpha = 10^{o}$, $\eta_1 = 0$ after the abrupt start

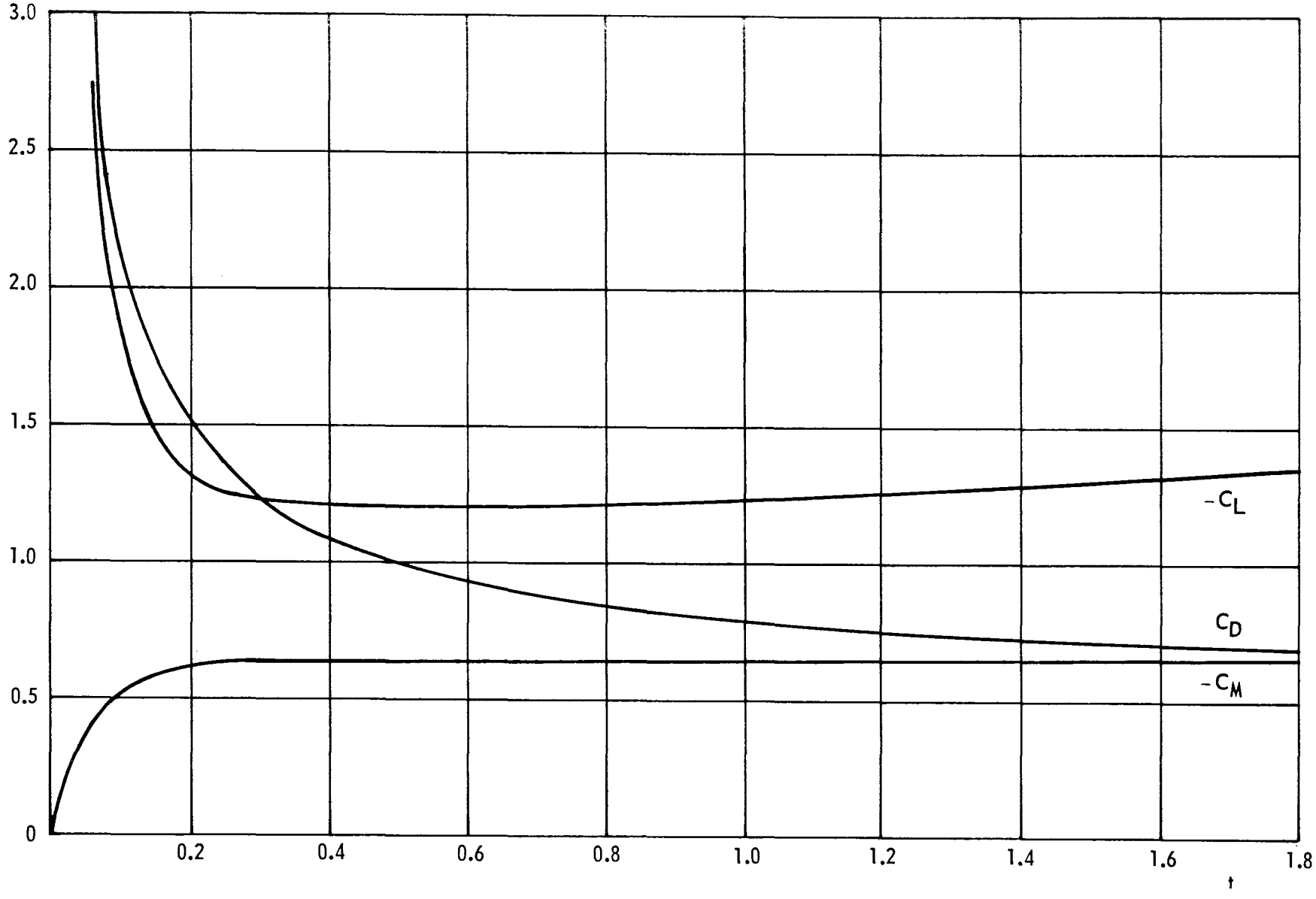

Figure 18 - Drag, lift, and moment coefficients versus time for Re = 200, $\alpha = 10^{\circ}$, $\eta_1 = 0$ after the abrupt **start**

for this small α-value but at much higher Reynolds number, does not occur in the present example.

For Re = 30, $\alpha = 45^{\circ}$, $\eta_1 = 0.1$ numerical results are obtained up to t = 16. Neither a clear development of a Kármán vortex street nor a tendency towards a steady state can be observed. The streamline patterns in Figure 19 show vortex shedding. However, the corresponding lines of constant vorticity do not exhibit local extrema; they only oscillate. Apparently, diffusion of vorticity at this low Reynolds number is already so dominant that vorticity extrema do not develop. Whether an oscillating state or a steady state is approached when $t \to \infty$ cannot be determined. However, the critical Reynolds number which separates these two states must be close to Re = 30. (For bodies normal to the flow the critical Reynolds number is higher and is about 45.) Figure 20 shows the coefficients C_{DF} and C_{LF} as functions of time.

The case Re = 15, $\alpha = 45^{\circ}$, $\eta_1 = 0.1$ is computed up to t = 7. Although a steady state is expected for $t \to \infty$, the time t = 7 is too small to be considered as giving an almost-steady state. At least a qualitative picture of the flow patterns is displayed in Figure 21. Additional information is recorded in Figures 22 and 23.

CONCLUSIONS

Computer simulation of vortex and vorticity shedding is possible with accuracy of the order of water- or wind-tunnel experiments for two-dimensional flows around bodies. With the space increments and

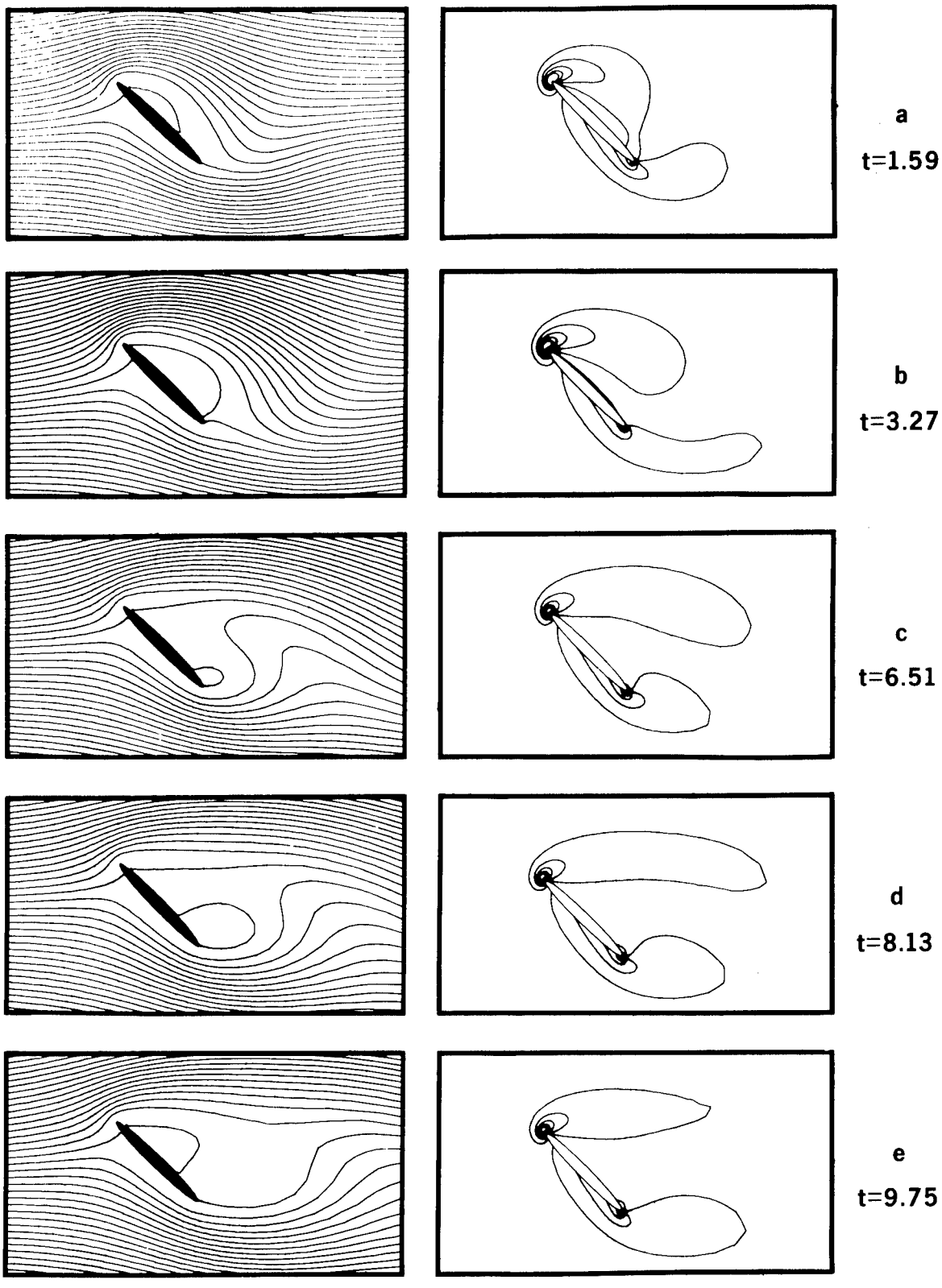

Figure 19 - Sequence of streamlines and equal-vorticity lines for Re = 30, $\alpha = 45^{\circ}$, $\eta_1 = 0.1$ at various times after the abrupt start. Potential flow at $t = 0$

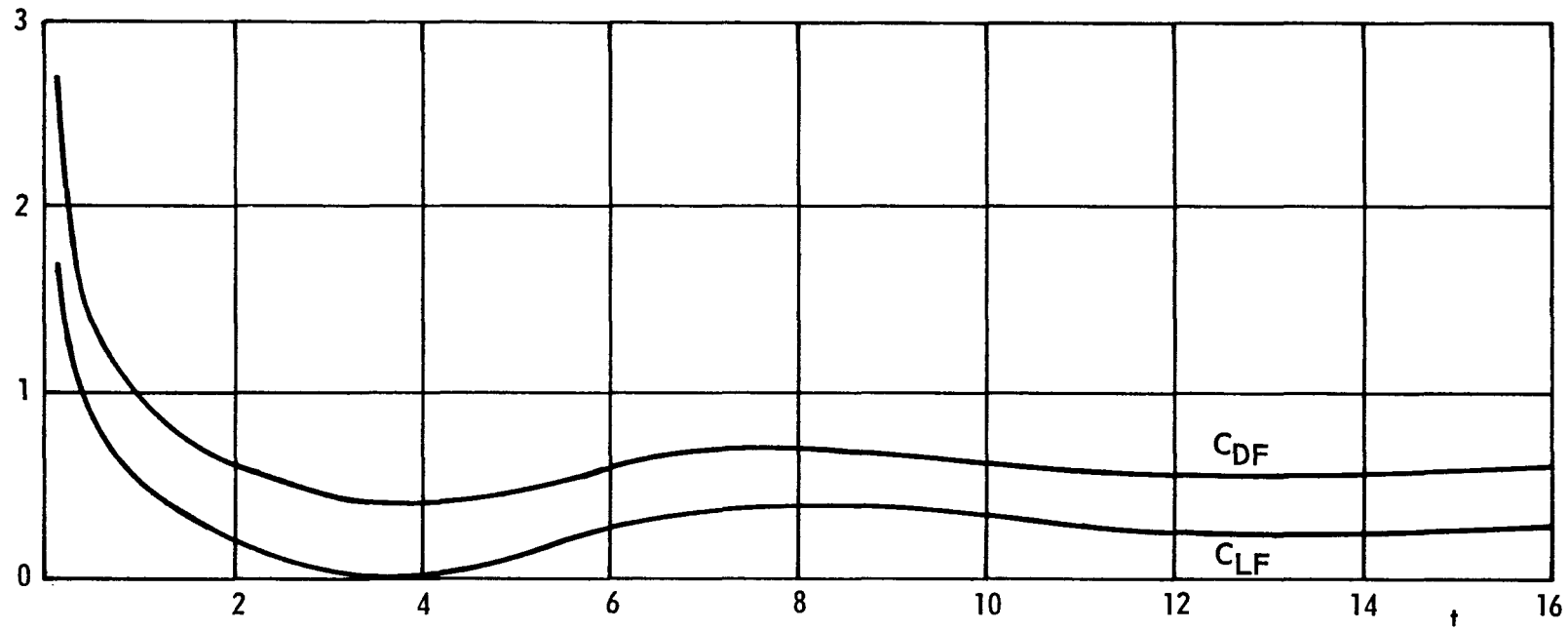

Figure 20 - Coefficients for frictional drag and lift versus time for Re = 30, $\alpha = 45^{\circ}$, $\eta_1 = 0.1$ after the abrupt start

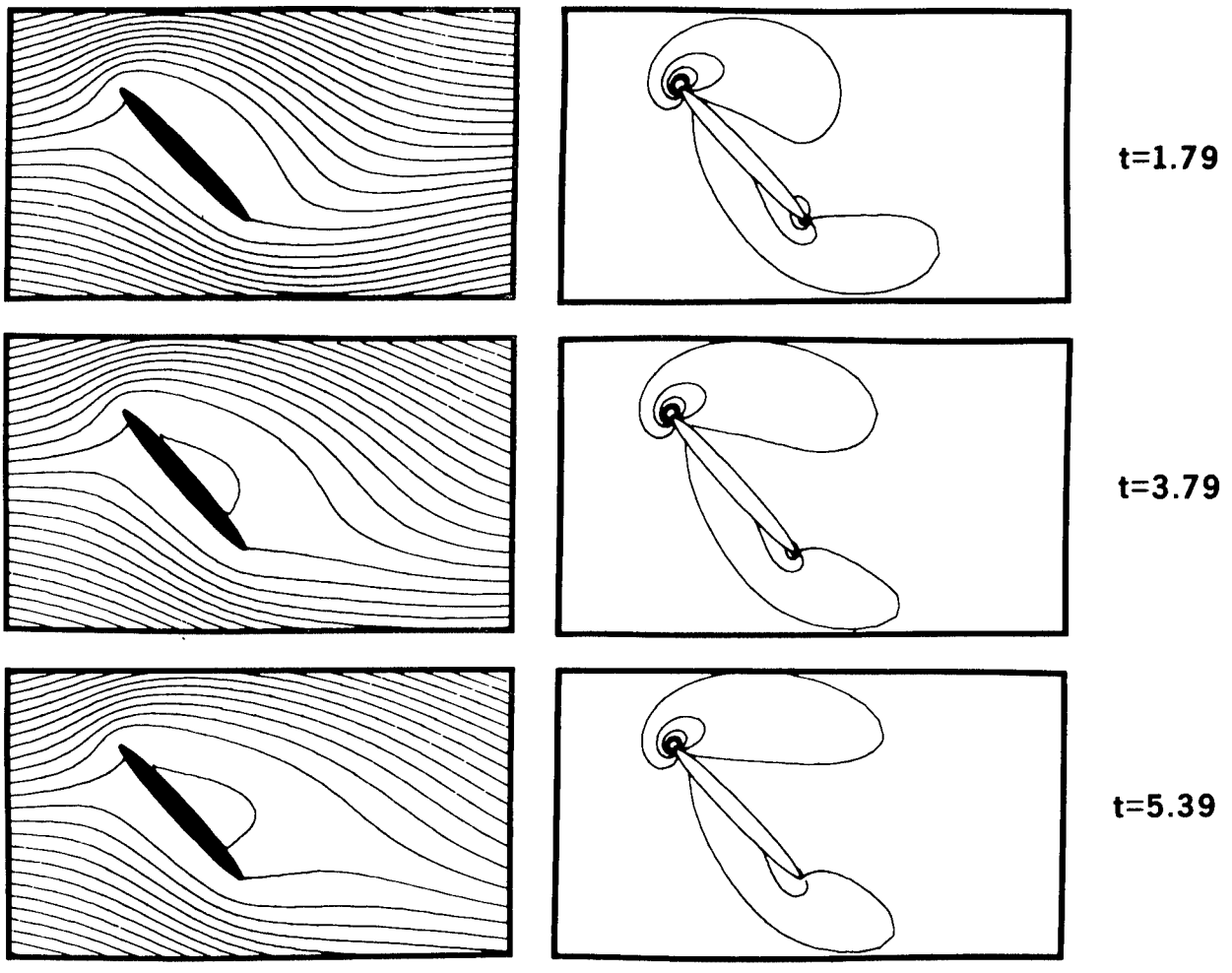

Figure 21 - Some patterns of streamlines and equal-vorticity lines for Re = 15, $\alpha = 45^{\circ}$, $\eta_1 = 0.1$ after the abrupt start

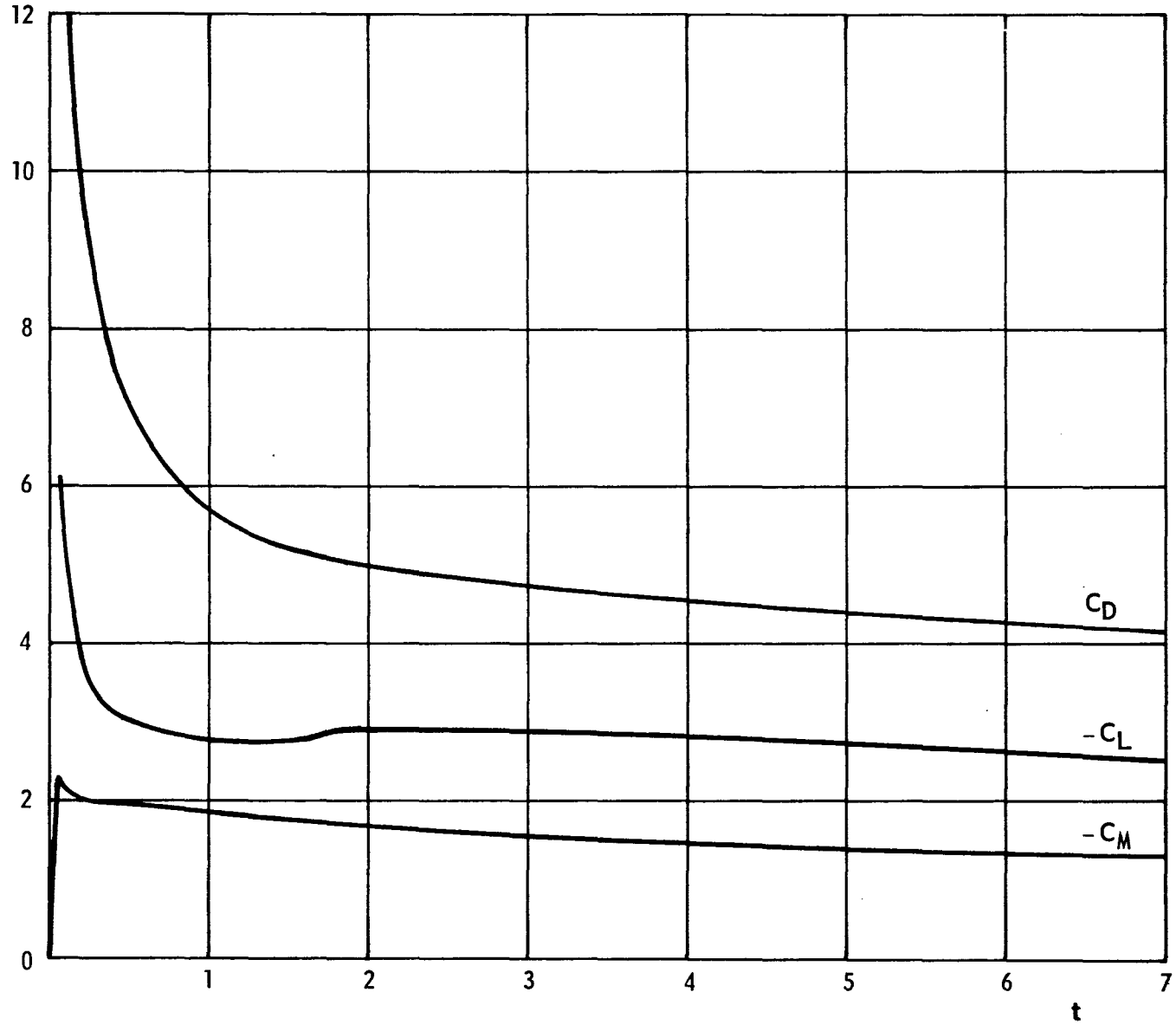

Figure 22 - Drag, lift, and moment coefficients versus time for Re = 15, $\alpha = 45^{\circ}$, $\eta_1 = 0.1$ after the abrupt start

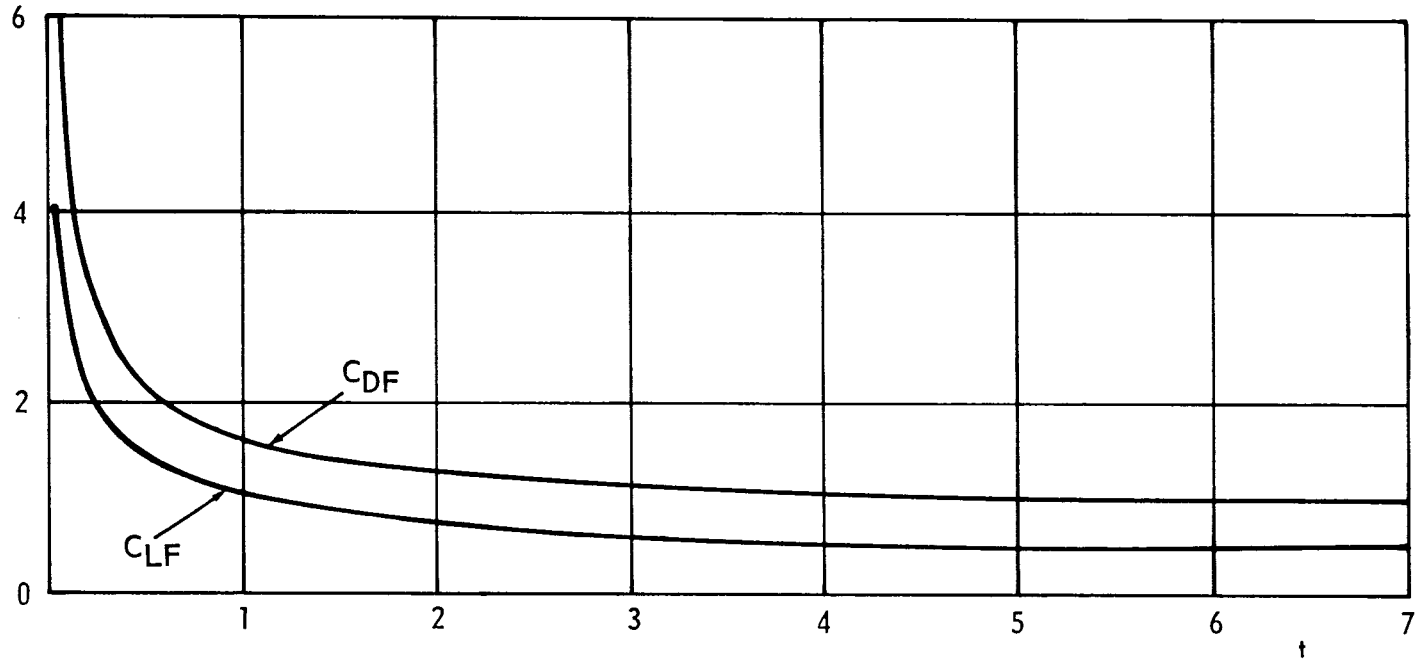

Figure 23 - Coefficients for frictional drag and lift versus time for Re = 15, $\alpha = 45^{\circ}$, $\eta_1 = 0.1$ after the abrupt start

number of grid points (75 x 60 or 75 x 80) used in this paper, the Reynolds number is limited to about 300. The flow region far from the body is not well represented. Improvements must be made in accuracy and in economy of computer time. Promising studies are under way.

The sudden start of a thin elliptic cylinder under an oblique angle of attack produces an initial vortex which separates from the trailing edge. After this time the zero streamline of the wake leaves the body parallel to the major axis at the trailing edge. This phenomenon, although occurring at Re = 200, verifies the soundness of the Lanchester-Prandtl hypothesis of potential flow, in which a circulation, necessary for the existence of lift, is postulated and determined by means of the Kutta condition.

For a thin elliptic cylinder with $\alpha = 45^{\circ}$ the lower limit of vortex shedding appears to be about Re = 30. (For symmetric configurations normal to the flow the lower limit is about Re = 45.)

All vortices shed from the body dissipate in such a way that the relative extrema of their vorticity (which may be considered as vortex centers) decrease in value approximately as 1/(t - const). Hence, they behave like decaying potential vortices when separated from the body.

ACKNOWLEDGMENT

The authors would like to thank Mr. S. Ohring for his help in running the computer program.

REFERENCES

1. Janssen, E., "Flow Past a Flat Plate at Low Reynolds Numbers," Journ. Fluid Mech. 3 (1957), 329.

2. Fromm, J.E. and Harlow, F.H., "Numerical Solution of the Problem of Vortex Street Development," Phys. Fluids 6 (1963), 975.

3. Dennis, S.C.R., and Dunwoody, J., "The Steady Flow of a Viscous Fluid Past a Flat Plate," Journ. Fluid Mech. 24 (1966), part 3, 577.

4. Dennis, S.C.R., and Chang, G., "Numerical Integration of the Navier-Stokes Equations for Steady Two-Dimensional Flow," Phys. Fluids Suppl. II, 1969, II-88.

5. Pao, Y., and Daugherty, R.J., "Time-Dependent Viscous Incompressible Flow Past a Finite Flat Plate," Boeing Scientific Research Lab., D1-82-0822, January 1969.

6. Wirz, H.J., "Die laminare Umströmung einer nichtangestellten Platte bei großen Reynoldszahlen," Doctoral Thesis, Technische Universität Berlin, 1971.

7. Dumitrescu, D. und Cazacu, M.D., "Theoretische und experimentelle Betrachtungen über die Strömung zäher Flüssigkeiten um eine Platte bei kleinen und mittleren Reynoldszahlen," Zeitschrift für angewandte Mathematik und Mechanik 50 (1970), 257.

8. Hirota, I., and Miyakoda, Journ. Meteor. Soc. Japan, Ser. II, 45, 30 (1965).

9. Thoman, D.C., and Szewczyk, A.A., "Numerical Solutions of Time-dependent Two-dimensional Flow of a Viscous, Incompressible Fluid over Stationary and Rotating Cylinders," Heat Transfer and Fluid Mechanics Laboratory, University of Notre Dame, Tech. Rep. 66-14, July 1966.

10. Jain, P.C., and Rao, K.S., "Numerical Solution of Unsteady Viscous Incompressible Fluid Flow Past a Circular Cylinder," Phys. Fluids Suppl. II, 1969, II-57.

11. Dawson, C., and Marcus, M., "DMC - A Computer Code to Simulate Viscous Flow About Arbitrarily Shaped Bodies," Proc. 1970 Heat Transfer and Fluid Mechanics Institute, Stanford University Press, (1970), 323.

12. v. Krzywoblocki, M.Z., "Vortex Streets in Fluids," Applied Mechanics Surveys, edited by M.N. Abramson et al., Spartan Books, Washington, D.C., 1966, 885.

13. Morkovin, M.V., "Flow Around Circular Cylinder - A Kaleidoscope of Challenging Fluid Phenomena," Symposium on Fully Separated Flows, 1964. The American Society of Mechanical Engineers, p. 102.

14. Lugt, H.J., and Schwiderski, E.W., "Flows Around Dihedral Angles," Proc. Roy. Soc. A 285 (1965), 382.

15. Schwiderski, E.W., Lugt, H.J., and Ugincius, P., "Axisymmetric Viscous Fluid Motions Around Conical Surfaces," Journ. SIAM 14 (1966), 191.

16. Rimon, Y., and Lugt, H.J., "Laminar Flows Past Oblate Spheroids of Various Thicknesses," Phys. Fluids 12 (1969), 2465.

17. Lugt, H.J., and Ohring, S., "Laminar Flows Past an Infinitely Thin Disk," Naval Ship Research and Development Center, Washington, D.C., Rep. No. 3654, 1971.

18. Rimon, Y., "Numerical Solution of the Incompressible Time-Dependent Viscous Flow Past a Thin Oblate Spheroid," Phys. Fluids Suppl. II, 1969, II-65.

19. Fromm, J.E., "Practical Investigation of Convective Difference Approximations of Reduced Dispersion," Phys. Fluids Suppl. II, 1969, II-3.

20. Briley, W.R., and Walls, H.A., "A Numerical Study of Time-Dependent Rotating Flow in a Cylindrical Container at Low and Moderate Reynolds Numbers," Lecture Notes in Physics, No. 8, Springer-Verlag, 1971.

21. Buzbee, B.L., Golub, G.H., and Nielson, C.W., "On Direct Methods for Solving Poisson's Equations," SIAM J. Num. Anal. 7 (1970), 627.

22. Lugt, H.J., and Rimon, Y., "Finite-Difference Approximations of the Vorticity of Laminar Flows at Solid Surfaces," Naval Ship Research and Development Center, Washington, D.C., Rep. No. 3306, 1970.

23. Lugt, H.J., and Haussling, H.J., "Transient Ekman and Stewartson Layers in a Rotating Tank with a Spinning Cover," Proceedings International Union of Theoretical and Applied Mechanics Symposium on Unsteady Boundary Layers, Quebec, 1971.

24. Taneda, S., "Standing Twin-Vortices behind a Thin Flat Plate Normal to the Flow," Research Institute for Applied Mechanics, Kyushu University, XVI, No. 54, 1968, 155.

25. Taneda, S., and Honji, H., "Unsteady Flow Past a Flat Plate Normal to the Direction of Motion," Journ. Phys. Soc. Japan 30 (1971), 262.

26. Timme, A., "Über die Geschwindigkeitsverteilung in Wirbeln," Ing. Archiv 25 (1957), 205.

27. Lugt, H.J., "The Spectrum of the Final Decay of Localized Disturbances in a Viscous Fluid," Naval Ship Research and Development Center, Washington, D.C., Rep. No. 2785, June 1968.

INITIAL DISTRIBUTION

Copies

1 DNL

7 CHONR
- 1 Dr. P. King (102)
- 1 Mr. M. Cooper (430B)
- 1 Dr. L. D. Bram (432)
- 1 Dr. R. D. Ryan (434)
- 1 Dr. B. J. Macdonald (436)
- 1 Mr. R. D. Cooper (438)

1 NRL, Tech Lib

4 NAVSHIPSYSCOM
- 1 SHIPS 031
- 1 SHIPS 0311
- 2 SHIPS 2052

1 NELC, Tech Lib

1 NOL

1 NAVUSEARANDCEN, Tech Lib

1 NAVWPNSCEN, Tech Lib

7 NWL
- 1 Mr. B. Smith (D)
- 1 Dr. C. J. Cohen (K)
- 1 Dr. A. V. Hershey (KXH)
- 1 Dr. E. W. Schwiderski (KXS)
- 1 Dr. P. Ugincius (KXU)
- 1 Dr. B. Zondek (KXZ)
- 1 Tech Lib

2 SUPT, USNA
- 1 Dept of Math
- 1 Lib

4 SUPT, PGSCHOL, Monterey
- 1 Lib, Tech Reports Sec
- 1 Math Dept
- 1 Dr. T. H. Gawin
- 1 Prof. T. Sarpkaya

Copies

1 ROTC & NAVADMINU, MIT

1 Naval War College

1 NAVSHIPYD BREM

1 NAVSHIPYD BSN

1 NAVSHIPYD CHASN

1 NAVSHIPYD HUNTERS PT

1 NAVSHIPYD LBEACH

1 NAVSHIPYD MARE ISLAND

1 NAVSHIPYD NORVA

1 NAVSHIPYD PEARL

1 NAVSHIPYD PHILA

1 NAVSHIPYD PTSMH

12 DDC

2 U. S. Army Math Res Ctr, Univ of Wisconsin, Madison
- 1 Dr. D. Greenspan
- 1 Tech Lib

1 U. S. Army Res. Off, Durham, N. C. 27706 CRD-AA-IPL Box CM

1 NASA, Washington, D. C.
- 1 Tech Lib

1 NASA, Marshall Space Flight Ctr, Huntsville, Ala 35809
- 1 Tech Lib

Copies

1 NASA, Lewis Res Ctr.
Cleveland, Ohio 44121

3 NASA, Ames Res Ctr,
Moffet Field, Calif 94305
1 Dr. W.J. McCroskey
1 Dr. E.D. Martin
1 Tech Lib

1 NASA, Langley Field
Tech Lib

4 Los Alamos Sci Lab,
Los Alamos, New Mexico
87544
1 Dr. F.H. Harlow
1 Dr. C.W. Hirt
1 Dr. B.J. Daly
1 Tech Lib

2 Brookhaven Nat Lab, Upton,
Long Island, N.Y.
1 Dr. P. Michael
1 Tech Lib

3 National Bureau of Standards
1 Dr. H. Oser
1 Dr. W. Sadowski
1 Tech Lib

2 Nat Sci Foundation,
1520 H St., N.W.
Washington, D.C. 20550
1 Engin Sci Div
1 Math Sci Div

4 Princeton Univ
1 Prof. S. I. Cheng
1 Dr. J. Smagorinsky
1 Dr. K. Bryan
1 Prof. M. Kruskal
1 Aerospace & Mech Eng Lib

1 USAEC, Tech Lib

Copies

2 Harvard Univ
1 Prof. G. Birkhoff
1 Prof. F.G. Carrier

4 MIT, Cambridge, Mass
1 Prof. J.G. Charney
1 Prof. C.C. Lin
1 Prof. S.A. Orszag
1 Prof. H.P. Greenspan

3 Univ of Md, College Park
1 Prof. A.J. Faller
1 Prof. A. Plotkin
1 Prof. D. Sallet

1 Oak Ridge Nat Lab.
Tech Lib

3 Courant Inst of Math Sci,
N.Y.U, N.Y., N.Y.
1 Prof. H.B. Keller
1 Dr. A.J. Chorin
1 Dr. Burstein

2 Stanford Univ
1 Prof. A. Acrivos
1 Prof. M.D. Van Dyke

3 Brown Univ, Prov., R.I.
1 Prof. W. Prager
1 Prof. J. Kestin
1 Prof. M. Sibulkin

2 Poly Inst of Brooklyn
1 Prof. G. Moretti
1 Prof. R.C. Ackerberg

3 Nat'l Cntr for Atmospheric
Res, Boulder, Colorado
80301
1 Dr. D.K. Lilly
1 Dr. A. Kasahara
1 Dr. J.W. Deardorff

Copies

1 Prof. J.S. Allen, Penn St Univ, Dept of Aerospace Eng, Univ Pk, Pa 16802

1 Dr. J.E. Fromm Dept 977, Bldg 025, Res Div, IBM Corp, Monterey and Cottle Road, San Jose, Calif 95114

1 Dr. C.W. van Atta Univ of Calif, La Jolla, Calif 92037

1 Dr. E.R. van Driest North American Rockwell Corp. 350 So. Magnolia Ave, Long Beach, Calif 90802

1 Prof. W.W. Wilmarth Univ of Mich, 1077 E. Engin Bldg, Ann Arbor, Mich 48104

1 Univ of Notre Dame
1 Prof. A.A. Szewczyk

2 West Virginia Univ Morgantown, West Virginia
1 Prof. J.B. Fanucci
1 Prof. W. Squire

1 Dr. D. Thoman C23 E. Mishawaha Ave, Mishawaha, Indiana

1 Prof. Z. Lavan Illinois Inst of Tech Chicago, Illinois 60616

1 Prof. K.E. Torrance Cornell Univ, Ithaca, N.Y.

1 Prof. M.Z. v. Krzywoblocki Mich St. Univ, East Lansing, Mich

Copies

1 Dr. W.E. Langlois IBM Res Lab, San Jose Calif

1 Prof. J. Happel Dept Chem Engr, N.Y.U., N.Y., N.Y.

1 Hq., American Society of Naval Engineers, 1012 14th St., N.W. Washington, D.C. 20005

1 Dr. M.V. Morkovin Dept Mech & Aerospace Engr, Ill Inst of Tech Chicago, Illinois 60616

1 Dr. Vivian O'Brien The Johns Hopkins Univ Applied Physics Lab 8621 Georgia Ave, Silver Spring, Md 20910

1 Prof. James C. Wu School of Aerospace Engr, Georgia Inst of Tech, Atlanta, Georgia 30332

1 Prof. E.V. Laitone Div of Aeronautical Sci Univ of Calif, Berkeley 94720

1 Prof. R.E. Goodson Purdue Univ, Automatic Control Cntr, School of Mech Engr, Lafayette, Indiana 47907

1 Mr. Stanley K. Jordan The Analytic Sciences Corp., 6 Jacob Way, Reading, Mass 01867

CENTER DISTRIBUTION

Copies	
1	01
1	15
1	154
1	154'
1	16
1	18
1	1802.2
100	1802.3
1	1805
1	184
5	1843
2	1892

UNCLASSIFIED
Security Classification

DOCUMENT CONTROL DATA - R & D

(Security classification of title, body of abstract and indexing annotation must be entered when the overall report is classified)

1. ORIGINATING ACTIVITY (Corporate author)

Naval Ship R&D Center
Bethesda, Maryland 20034

2a. REPORT SECURITY CLASSIFICATION
UNCLASSIFIED

2b. GROUP

3. REPORT TITLE

LAMINAR FLOWS PAST ELLIPTIC CYLINDERS AT VARIOUS ANGLES OF ATTACK

4. DESCRIPTIVE NOTES (Type of report and inclusive dates)

5. AUTHOR(S) (First name, middle initial, last name)

Hans J. Lugt and Henry J. Haussling

6. REPORT DATE
February 1972

7a. TOTAL NO. OF PAGES
61

7b. NO. OF REFS
27

8a. CONTRACT OR GRANT NO.

b. PROJECT NO. ZR 011 01 01
SR 014 03 01

c.

d.

9a. ORIGINATOR'S REPORT NUMBER(S)

3748

9b. OTHER REPORT NO(S) (Any other numbers that may be assigned this report)

10. DISTRIBUTION STATEMENT

Approved for public release; distribution unlimited.

11. SUPPLEMENTARY NOTES

12. SPONSORING MILITARY ACTIVITY

NAVMAT, NAVSHIPS

13. ABSTRACT

Numerical solutions for laminar incompressible fluid flows past thin elliptic cylinders at various angles of attack are obtained using a stream function-vorticity formulation. The flow is considered to be two-dimensional and time-dependent. Potential flow is selected as the initial condition. Almost steady-state solutions have been computed for the cases $\alpha = 0^{o}$, Re = 200; $\alpha = 45^{o}$, Re = 15; and $\alpha = 90^{o}$, Re = 10 where α and Re are the angle of attack and the Reynolds number, respectively. Vortex shedding has been studied for $\alpha = 45^{o}$, Re = 30 and 200.

DD FORM 1 NOV 65 1473 (PAGE 1)

S/N 0101-807-6801

UNCLASSIFIED
Security Classification

14 KEY WORDS	LINK A ROLE	LINK A WT	LINK B ROLE	LINK B WT	LINK C ROLE	LINK C WT
Navier-Stokes equations						
Vortex shedding						
Finite-difference method						
Flow past plate						